Carbon Nanomaterials as Electrodes for Lithium-Ion Batteries - A Computational Study

Raul Ekberg Dias
Master in Chemistry
Department of Chemistry and Biochemistry
Faculty of Sciences of the University of Porto
2024

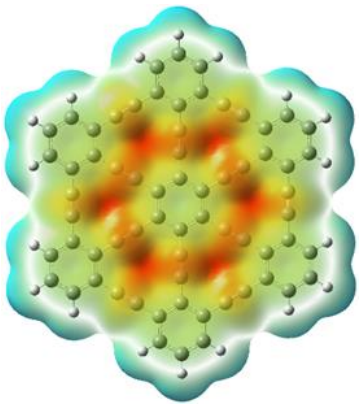

Carbon Nanomaterials as Electrodes for Lithium-Ion Batteries - A Computational Study

Raul Ekberg Dias

Dissertation
Master in Chemistry
Faculty of Sciences of the University of Porto
Department of Chemistry and Biochemistry
2024

Supervisor
Alexandre Lopes Magalhães, Professor auxiliar,
Faculty of Sciences of the University of Porto

Aos meus pais

Agradecimentos

Esta dissertação representa a conclusão dos trabalhos acadêmicos que iniciei ao concluir a Licenciatura, dois IJUPs, uma conferência, um artigo publicado e outro em desenvolvimento. Sinto-me grato e orgulhoso por todo o percurso que trilhei até aqui.

Primeiramente, agradeço à Faculdade de Ciências da Universidade do Porto e a todo o seu corpo docente, especialmente ao meu orientador, Professor Alexandre Magalhães. Sou profundamente grato por toda a ajuda e mentoria ao longo desses anos, desde a minha Licenciatura até o Mestrado. Diante de cada problema que surgia no meu caminho acadêmico, sempre encontrava tranquilidade após conversar com o Professor, independentemente da gravidade dos obstáculos, pois sabia que, juntos, encontraríamos uma solução.

Agradeço também a todos os meus amigos, tanto no Brasil quanto em Portugal. Em especial, expresso minha gratidão aos amigos Thiago Marcon e Maria Eduarda Vieira, com quem passei grande parte do meu tempo. Sempre pude confiar neles, assim como estive presente para apoiá-los.

Por fim, agradeço aos meus pais e ao meu irmão, que sempre estiveram ao meu lado. Destaco o apoio incondicional dos meus pais, que mesmo vivendo no Brasil, me ofereceram tudo o que podiam. Sempre pude matar a saudade com as suas estadias em Portugal e as nossas viagens pelo antigo continente.

Resumo

As baterias de ião-lítio (LIBs) tornaram-se uma parte vital das soluções de armazenamento de energia no mundo nas últimas décadas, principalmente nos mercados de pequenos eletrónicos e veículos elétricos. A densidade energética do lítio e as propriedades eletrônicas do grafeno os tornaram uma combinação perfeita, sendo amplamente utilizados nas LIBs mais comuns atualmente. Nos últimos anos, outros nanomateriais como o grafino surgiram como candidatos altamente promissores para o desenvolvimento de designs de elétrodos inovadores. Com base nisso, este estudo investigou e analisou, por meio de cálculos da teoria do funcional da densidade (DFT), diferentes compostos de grafeno e grafino para avaliar suas capacidades como potenciais candidatos a serem implementados em LIBs.

Sendo assim, 29 diferentes compostos de grafeno e 63 diferentes compostos de grafino, com e sem substituintes, foram revisados com base em suas propriedades eletrónicas para verificar sua aptidão como cátodos para LIBs. Um total de doze substituintes foram estudados neste projeto, sendo eles os grupos carbonilo, fluoreto, cloreto, hidroxilo, amino, nitrilo, nitro, carboxilo, triclorometil, trifluorometil, sulfeno e dimetilamino.

Uma forte correlação entre o potencial redox dos compostos substituídos e sua afinidade eletrónica foi estabelecida, o que possibilita o uso de uma metodologia menos intensiva em termos computacionais. Os resultados demonstram claramente que a natureza, o número e o posicionamento relativo dos substituintes desempenham um papel decisivo na determinação das propriedades dos elétrodos. Notavelmente, os grupos funcionais nitro e carbonilo resultaram em aumentos mais promissores de potencial tanto no grafeno quanto no grafino, enquanto o grupo nitrilo mostrou leve aumento no grafeno, e o trifluorometil mostrou melhorias no sistema do grafino.

Palavras-chave: bateria de ião-lítio (LIB), grafeno, grafino, nanomaterial de carbono, teoria do funcional da densidade (DFT), potencial redox, carga superficial, análise de correlação

Abstract

Lithium-ion batteries (LIBs) have become a vital part of the world's energy storage solutions in the last decades, mostly in the small electronics and electric vehicles markets. Lithium energy density properties and graphene's electronic properties made them a perfect pair that is used in most common LIBs today. In recent years, other nanomaterials like graphyne have emerged as highly promising candidates for developing innovative electrode designs. On that grounds, this study investigated and analyzed through density functional theory (DFT) calculations graphene and graphyne unique compounds to assess their capabilities as potential candidates to be implemented in LIBs.

Thus, 29 graphene unique compounds and 63 graphyne unique compounds with and without substituents were reviewed via their electronic properties to verify their aptitude as cathodes for LIBs. A total of twelve substituents were studied in this project being the carbonyl, fluoride, chloride, hydroxyl, amino, nitrile, nitro, carboxyl, trichloromethyl, trifluoromethyl, sulfeno and dimethylamino groups.

A strong correlation between the redox potentials of the substituted compounds and their electron affinity was established, that enables the use of a less computationally intensive methodology. The results clearly demonstrate that the nature, number, and relative positioning of the substituents play a decisive role in determining the electrode properties. Notably, the nitro and carbonyl functional groups resulted in the most promising enhancements to the potential of both graphene and graphyne, while the nitrile groups showed some improvement in graphene and the trifluoromethyl showed improvements in the graphyne system.

Keywords: lithium-ion battery (LIB), graphene, graphyne, carbon nanomaterial, density functional theory (DFT), redox potential, surface charge, correlation analysis

Table of Contents

List of Figures

List of Tables

List of Equations

List of Appendices

List of Abbreviations

CNT	CARBON NANOTUBE
DFT	DENSITY FUNCTIONAL THEORY
DMC	DIMETHYL CARBONATE
EC	ETHYLENE CARBONATE
EV	ELECTRIC VEHICLE
FCUP	FACULTY OF SCIENCES OF THE UNIVERSITY OF PORTO
HF	HARTREE-FOCK
IEFPCM	INTEGRATED EQUATION FORMALISM VARIABLE
LCAO	LINEAR COMBINATION OF ATOMIC ORBITALS
LIB	LITHIUM-ION BATTERY
MWCNT	MULTI-WALLED CARBON NANOTUBE
PC	PROPYLENE CARBONATE
PCM	POLARIZABLE CONTINUUM MODEL
SCF	SELF-CONSISTENT FIELD
SEI	SOLID ELECTROLYTE INTERPHASE
SHE	STANDARD HYDROGEN ELECTRODE
STO	SLATER-TYPE ORBITAL
UP	UNIVERSITY OF PORTO

Chapter I

Introduction

1. Lithium-Ion Battery

It is important to understand how a secondary lithium-ion battery (LIB) and each of its parts function to be able to predict, model and develop new components. In simple terms, a generic LIB can be divided into three zones (Fig. 1).

In the first zone and during the charging process of the battery, the lithium cathode sends electrons to the anode through a conductive metal and releases into the electrolyte solution positive lithium ions. Subsequently, lithium ions will be solvated by the electrolyte and transported by diffusion to the cathode. The electrolyte does not accept electrons, keeping a crucial barrier between the poles of the battery to deter from shorts. In the last zone, the lithium ions coming from the electrolyte bind to the anode and receive electrons by the cathode via the wires and conductive metal in which the anode is anchored. Also in the anode, there is an interface that extends the battery life called the solid electrolyte interphase (SEI) that is comprised of lithium, electrolyte molecules and the surface of the anode.

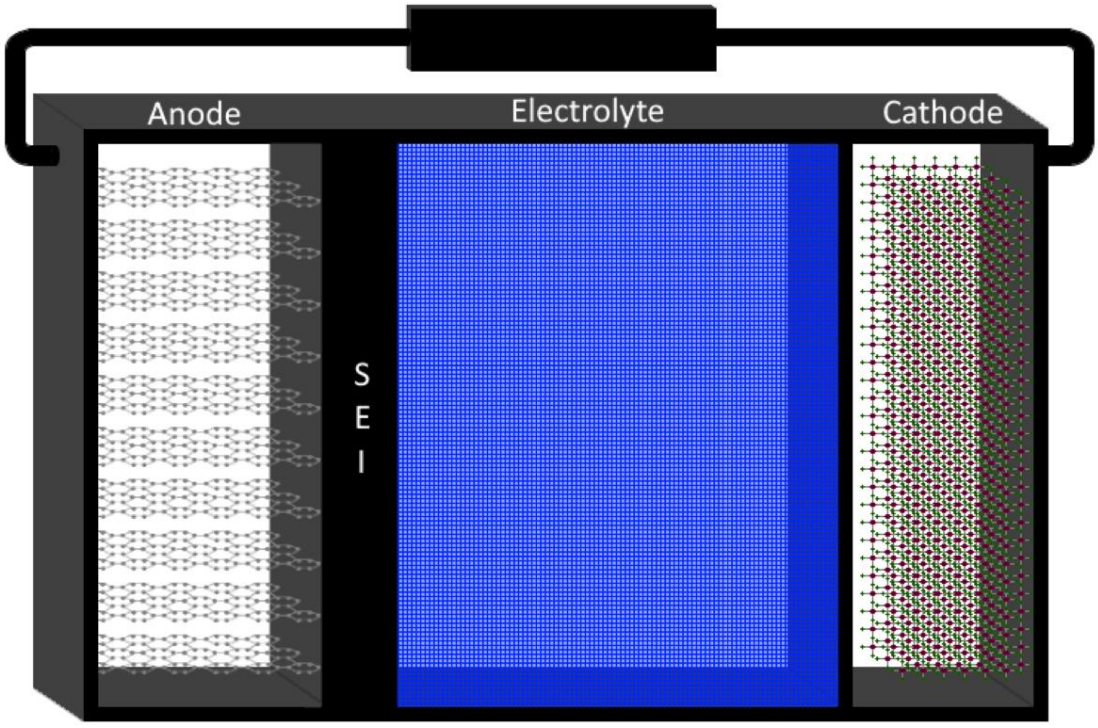

Figure 1: Representation of a simplified LIB with three distinct parts.

While the device is used, the spontaneous discharge process that happens can be seen as switching the polarity of the battery making the anode be the negative electrode that sends electrons to the positive lithium electrode via wiring and releasing into the electrolyte a lithium ion that will return to the cathode.

1.1. Battery technologies prior to lithium

In the late XVIII century, Alessandro Volta invented the voltaic pile, the first true electrical battery, by stacking alternating copper and zinc disks in a pile and soaking them in brine. When the top and bottom disks were connected by wires it allowed for the flow of electrons between the alternating anode and cathode layers soaked in the electrolyte solution [1]. Although it lacked a lot when put to use but, it showed what the power of energy storage could accomplish and with the help of other brilliant minds such as John Frederic Daniell who invented the Daniell cell in 1836, step by step battery technology was being improved and developed [2].

The first breakthrough in the field happened in 1859 when Gaston Planté invented the lead-acid battery, the first rechargeable battery that would become the first ever commercial battery. The first lead-acid cell consisted of two lead sheets rolled into spirals and placed inside a cylindrical container with a sulfuric acid solution. Unlike its predecessors, by reversing the current through the battery it was possible to recharge without needing to redo or rebuild the whole cell [3,4]. Up to this day, the contemporary Pb-acid type of batteries still has a sizeable chunk in the battery market [5].

At the turn of the 20th century, nickel-based batteries were invented by Ernst Waldemar Jungner using nickel oxyhydroxide (NiOOH) as the cathode and were paired with firstly iron (Ni-Fe) or cadmium (Ni-Cd) electrodes that together with zinc and hydrogen consist today of the most common combination in nickel-based batteries [6]. As early as 1910, Ni-Fe batteries were used to power electric vehicles (EVs) and Ni-Cd remain until today the selected choice for the aviation industry [7,8]. Later, some automotive manufacturers such as Toyota and Honda developed EVs using nickel metal hydride (Ni-MH) [9]. Unfortunately, since their invention, nickel-based batteries suffer from performance problems after continued cycles and poor thermal stability that are still to this day the focus of some researches [10,11].

1.2. Lithium-ion battery

Lithium (Li) appeared in the battery research field, in 1912, when scientist Gilbert N. Lewis began researching its capabilities since other alkaline batteries were also being tested [12]. Several decades later, primary LIBs were already available as commercial energy solutions in the late 1960s because of their high voltage, high energy density, low self-discharge rate, long storage lifetimes and wide temperature range [13,14]. Although this type of battery cannot be recharged, some fields such as deep space exploration and invasive permanent medical devices still use primary LIBs because connecting the device to an energy source can be difficult or even impossible. [15,16].

Before the first secondary LIBs appeared on the market, decades of research done brick by brick created the foundation of the LIB development that is credited mainly to scientist John B. Goodenough, M. Stanley Whittingham and Akira Yoshino who were awarded the Nobel Prize in Chemistry at 2019 for their prototype LIB that used $LiCoO_2$ and graphite as electrodes [17]. In 1991, Sony and their manufacturing partners introduced in one of their devices the 3.8 V average secondary LIB [18]. Ever since, the small portable electronic market and the EV market have majorly adopted Li as their choice for type of battery and propelled the academia to research and development of this technology. This demand for more efficient energy solutions forecasts a compound annual growth of 14.2% until 2032 in the global LIB marked size [19].

In recent years, extensive research into the development of new materials to improve batteries has rapidly progressed. Correspondingly, the development of promising anodes, such as fluorographenes and boron-doped graphenes [20–22], new electrolytes and solvents mixtures, such as those containing ethylene carbonate (EC), dimethyl carbonate (DMC), and propylene carbonate (PC) [23–26], as well as new cathodes, such as lithium iron phosphate and lithium bisulfate [27,28], have been investigated. Nowadays, graphene is present in most batteries due to its impressive electrical and thermal conductivity, flexibility, mechanical strength, stability, and the ability to bond with other elements to further enhance these and other properties [29,30]. Additionally, newer carbon-based nanomaterials such as graphyne have also been studied in this field because of their 2D unique type of structure and possible combinations of sp- and sp2-hybridized carbon atoms that lead to very promising properties like their increased storage capacity and other electronic and mechanical properties [31,32].

2. Carbon Nanomaterials

Few other elements have been researched as thoroughly and used in as many different areas of human society as carbon. Upon the valence bond theory, this fact can be ultimately attributed to a process called hybridization in which an atom goes to an excited state and combine its orbitals to better bond with other elements resulting in an overall energy gain because the energy barrier to excite the atom is small than binding energy [31,32].

An isolated neutral carbon atom has six electrons in which four of them are in the valence shell. The reduced energy gap between the 2s and 2p orbitals allows carbon to combine them up to three different hybridized orbitals (Fig. 2).

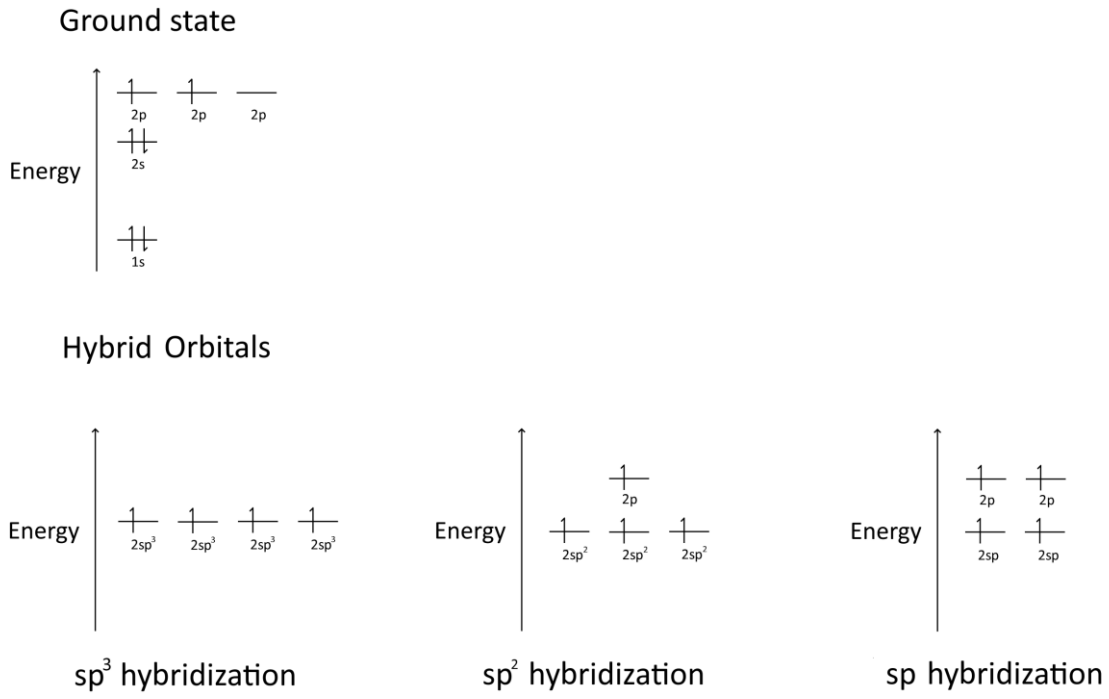

Figure 2: Electronic structure of a non-hybridized carbon atom and of different hybrid states.

While other elements also undergo hybridization [33], carbon atoms in one hybridized state can bond with carbon atoms in other hybridized states laying a foundation to creating an unmeasurable combination of molecules with vastly different properties. In addition, if other elements that can bond with carbon are accounted in this evaluation, then this makes it clear why carbon is so unique compared to the other elements.

A way to visualize the result of hybridization is by looking at the spatial orientations formed in carbon allotropes and nanostructures like diamond, graphite, carbon nanotubes (CNTs) and graphyne. The diamond has only sp^3 hybridized carbon atoms forming four 109°28′ angled tetrahedral bonds with other carbon atoms in all directions resulting in a single network that is only bonded by covalent interactions, thus resulting in a strong mechanical resistance [34]. Graphite is made of graphene sheets that are kept together in layers by π−π interactions [35], only able to covalent expand in one plane because the planar nature of the sp^2 hybridization. Graphyne contains both sp and sp^2 hybridization, having similar properties to graphene and only expanding in its plane. In the other hand, CNTs are formed by *quasi* sp^2 hybridized carbon atoms that are slightly angular deformed and can only expand in one axis, because of the folding process to form this structure (Fig. 3).

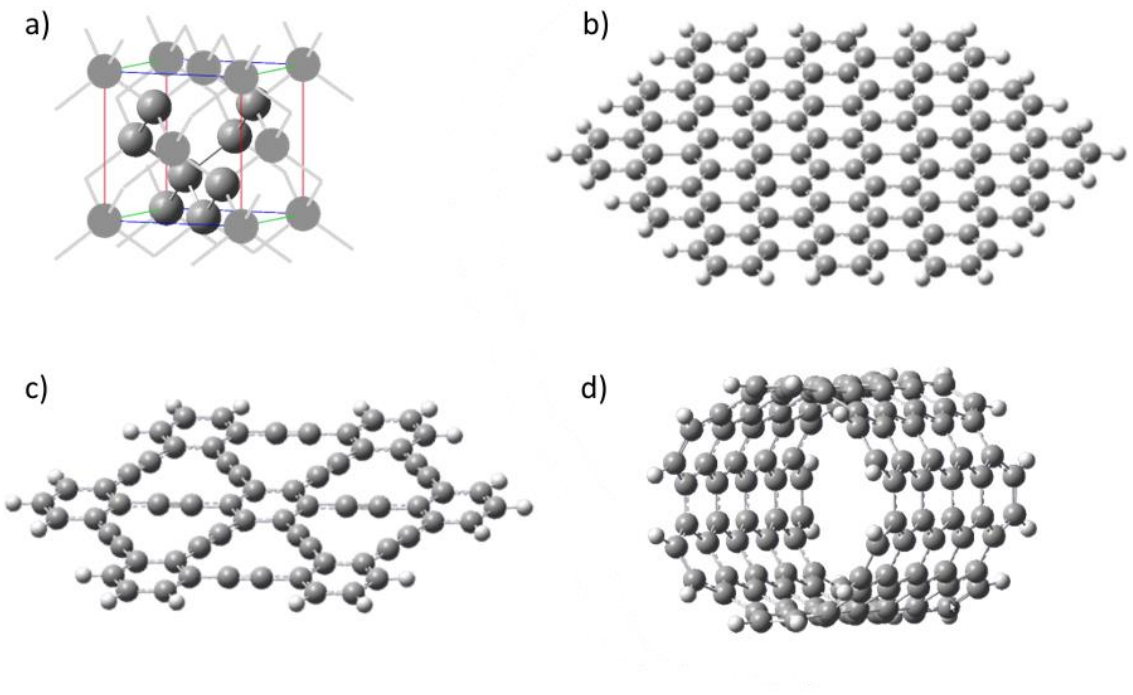

Figure 3: Finite representation of the structures of four carbon nanomaterials: a) diamond's unit cell, b) graphene, c) graphyne and d) carbon nanotube.

Furthermore, carbon nanomaterials such as graphene and graphyne exhibit anisotropic properties meaning that physical, chemical, electric and thermal properties are not the same in all directions. For that reason, their ability to accommodate partial charges, mechanical strength, disperse heat and other properties depend on the orientation. It is important to take this factor into account to design products with these types of materials.

2.1. Graphene

Although graphene has been studied theoretically for decades, it was only isolated in 2003 using a simple yet effective mechanical method with adhesive tape [36]. This led to even more studies and granted Andre Geim and Konstantin Novoselov the 2010 Physics Nobel Prize.

Graphene consists of a carbon atom monolayer material where each sp^2 carbon atom bonds with a 120° angle to three other carbon atoms that can extend the structure only in the plane forming a honeycomb structure. Similar to aromatic systems, the planar nature of graphene causes the combination of the π bonded orbitals of each carbon atom in the network for the creation of a delocalized π system [37], resulting in C-C bonds that exhibit characteristics between those of single and double bonds (Fig. 4).

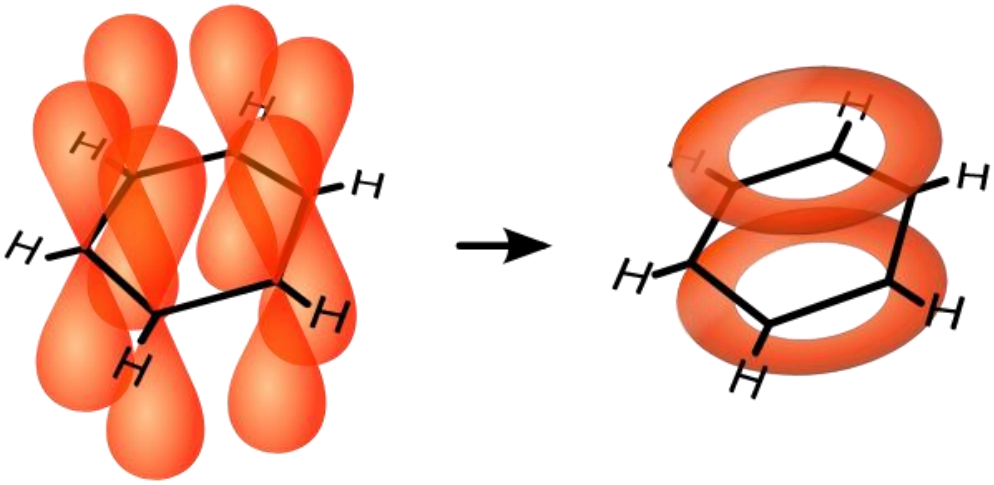

Figure 4: Illustration of the π orbital combination in benzene that forms a delocalized π system.

Graphene layers in graphite are mostly arranged in a pattern that repeats every second layer called Bernal stacking (Fig. 5a), in which carbon atoms in sheet A are horizontally separated from the carbon atoms of the neighbor B sheets by half of their orthogonal length. In this way, half of the carbon atoms of each ring are placed in between the empty spaces of the other layer's rings, consequently half of all carbon atoms in the network are found accordingly [32,38,39].

Even though the Bernal-stacked layout is believed to be the most stable because of its minimum energy configuration, there is plenty of other arrangements that occur like for example AA' (Fig. 5b) stacking that may favor multi-walled carbon nanotubes (MWCNTs) growth [40,41] and ABC stacking (Fig. 5c) found as a metastable state in natural graphite [32,42].

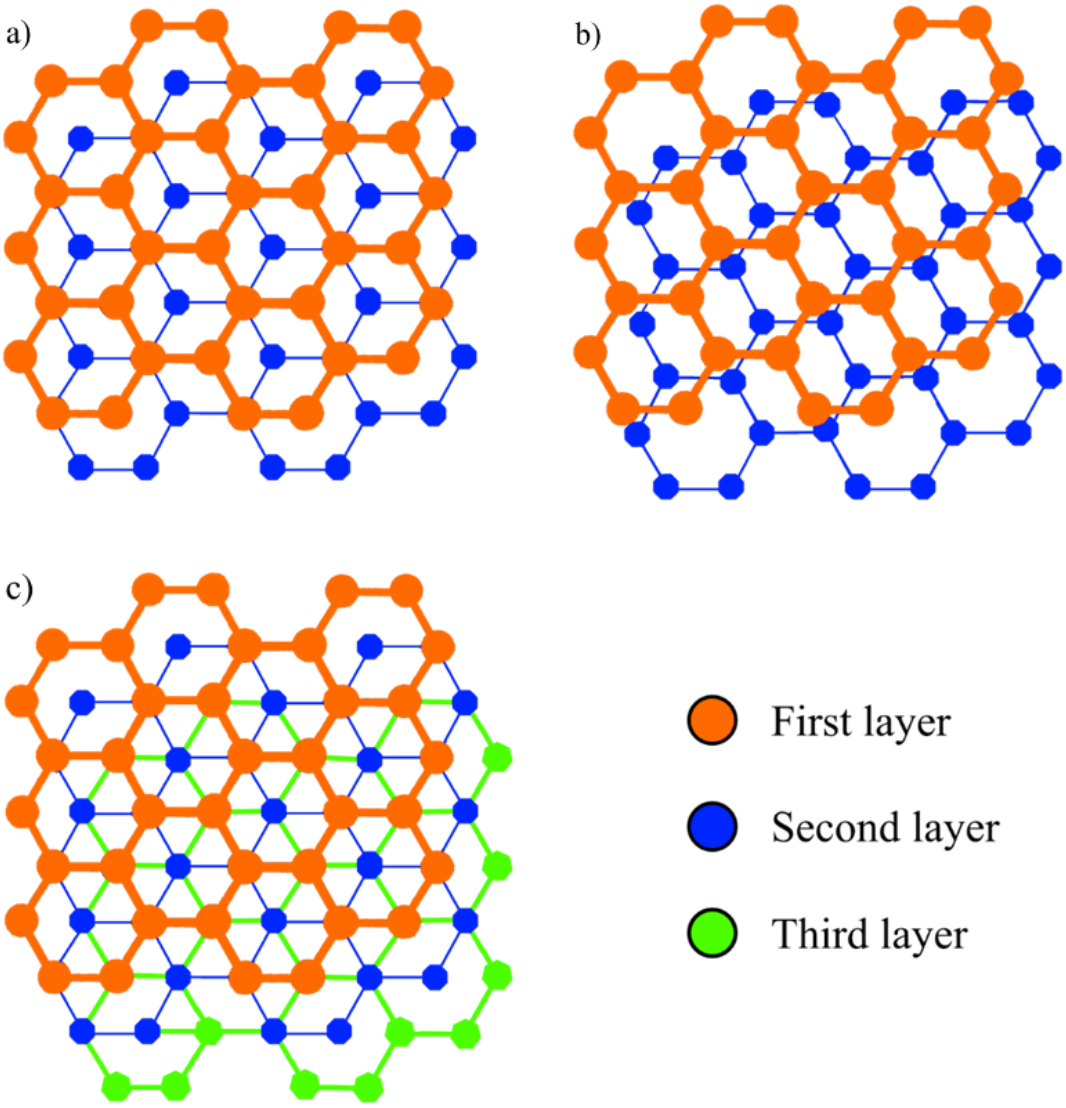

Figure 5: The graphite lattice structure for the a) AB pattern, b) AA' pattern and c) ABC pattern.

2.2. Graphyne

First theorized in 1987 by Baughman, Eckhardt, and Kertesz, the graphyne family of compounds are sp and sp^2-hybridized carbon atoms bonded in a graphene-like framework with varying types of combinations [43]. The first reproducible and successful graphyne synthesis was done in 2009 by Guoxing Li and his group, where they performed a Glaser–Hay cross-coupling reaction with hexaethynyl-benzene producing γ-graphdiyne nanoscale films [44].

The nomenclature for this group of materials is X-graph-n-yne, where X is the prefix for the different ways of combining sp and sp^2-hybridized carbon atoms that can α, β, and γ and n is the number of acetylene groups in the unit cell (Fig 6). Depending on the ratio of sp and sp2 hybrid carbon atoms in the network and the different ways of bonding them, it is possible to change properties like electronic transport, aromaticity and other properties [45,46].

The introduction of the acetylenic bonds when compared to graphene gives interesting physical and electronic properties like reducing the rigidity of the structure and lower Fermi velocities that make graphyne an even more compelling material to be applied in LIBs, H_2 storage and single atom catalysis [47].

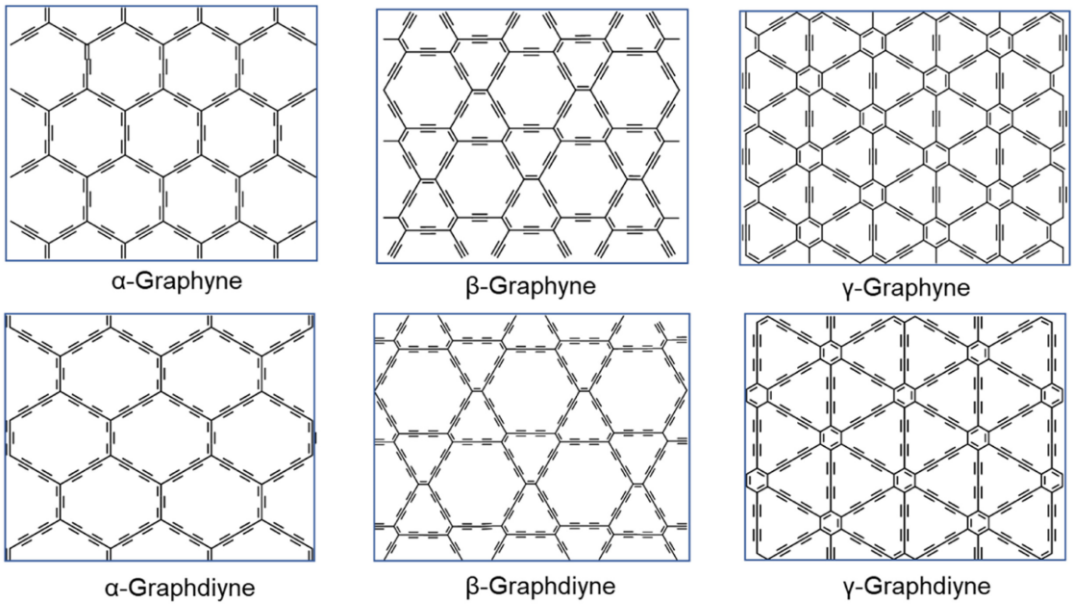

Figure 6: Different graphyne structures that can be formed by alternating the number and position of acetylenic bonds. Adapted from “Artificial carbon allotrope γ-graphyne: Synthesis, properties, and applications.,” by J. Li and Y. Han, 2023, *Giant*, *13*, 100140. Copyright 2023 by Elsevier [47].

Chapter II

Methodology

1. Quantum Mechanics

Quantum mechanics changed the understanding humanity had of the atomic and subatomic world. Research fields such as lasers, transistors, cryptography and innumerous others have benefited from its ripples that keep emerging up to this day. The following section serves to present and briefly explain the set of postulates in which quantum mechanics is based on [48,49].

Postulate 1 – The wave function postulate: The state of a system can be described as a wave function defined by spatial coordinates, spin coordinates and time. From this, it is possible to calculate the probability of finding the space-spin coordinates of a particle.

Postulate 2 – Operators for observable variables: Every observable property in a system corresponds to a linear Hermitian operator.

Postulate 3 – Measured values to eigenvalues: Any measurement of a dynamic variable is one of the eigenvalues of the corresponding operator. Thus, measured values can take any value of the allowed eigenvalues but not one outside of that.

Postulate 4 – The average values: The average value of observable can be described by an operator. This allows to calculate an average value of an observable variable in a large number of systems with the same state function.

Postulate 5 – The time-dependent Schrödinger equation: The wave function of a system will evolve in time according to the time-dependent Schrödinger equation if undisturbed.

Postulate 6 – The antisymmetric postulate: The total wave function of a system must be antisymmetric accounting for the electronic spin.

1.1. Development of quantum mechanics

In the late XIX century, scientists discovered that the light emitted by an object that absorbed all light also known as blackbody did not follow the expected patterns when using statistical mechanics and the electromagnetic-wave model of light. After almost a decade of research, Max Plank proposed the idea that the radiation emitted by the blackbody was quantized meaning that the energy E was given in amounts of $h \times \nu$ where ν is the radiation frequency and h is the Planck's constant.

$$E = h \times \nu \quad (1)$$

Almost a decade later, Ernest Rutherford developed an atomic model to better explain the atom structure after noticing deflations of charged particles when shot close to nuclei. The biggest problem of his model was the fact that by his theory the electrons would continuously lose energy until they spiral into the nucleus. In the following years, Niels Bohr came up with a hypothesis that was founded on the same principle of quantized energy which prevents the atomic collapse to happen. The electron would only have defined orbits and would emit or absorb a photon when changing the orbit and would explain the flaw in Rutherford's design.

Although Bohr solved this problem in Rutherford's atomic model, he could only apply and get correct predictions to hydrogenic systems and would fail when accounting for systems that had two or more electrons because of the roots in classical mechanics that this theory had. Later, in 1923, Louis de Broglie proposed that electrons behaved both as waves and particles after analyzing the results of his own and other contemporary scientists' experiments. The de Broglie wavelength equation stated that electrons have a wavelength aspect λ equal to the Planck's constant divided by its mass m and velocity V.

$$\lambda = \frac{h}{m \times V} \quad (2)$$

The last piece before the turning point came in 1927, Werner Heisenberg formulated the fundamental principal in which quantum mechanics would anchor by contemplating Davisson and Germer studies that were consistent with de Broglie theory. To understand this key point is important to refer to the double slit experiment (Fig. 7) where an electron beam would go through two plates with respectively one and two slits before reaching a light source would be positioned after the second plate and finally the screen. When only one of the slits of the second plate was closed, either one of them, it would show on the measuring screen one pattern coming from the slit that was open, thus making the electron act like a particle. However, when the electron beam passed through both open slits in the second plate it would show a diffraction pattern on the screen when the light source was turned off, thus proving that the electrons were behaving as a wave. By turning on the light, the photons affected the momenta of the electrons and a single pattern would show on the screen. When using a light source that would produce lower momentum photons, it would generate an increasing diffraction pattern on the screen the lower the photon momentum became, creating an uncertainty in which slit the electron passed through. Hence, to know through which slit the electron passed we need

to change its momentum to a value not known and to keep the momentum of the original beam the resulting diffraction pattern doesn't inform which slit the electron passed or in another word its position.

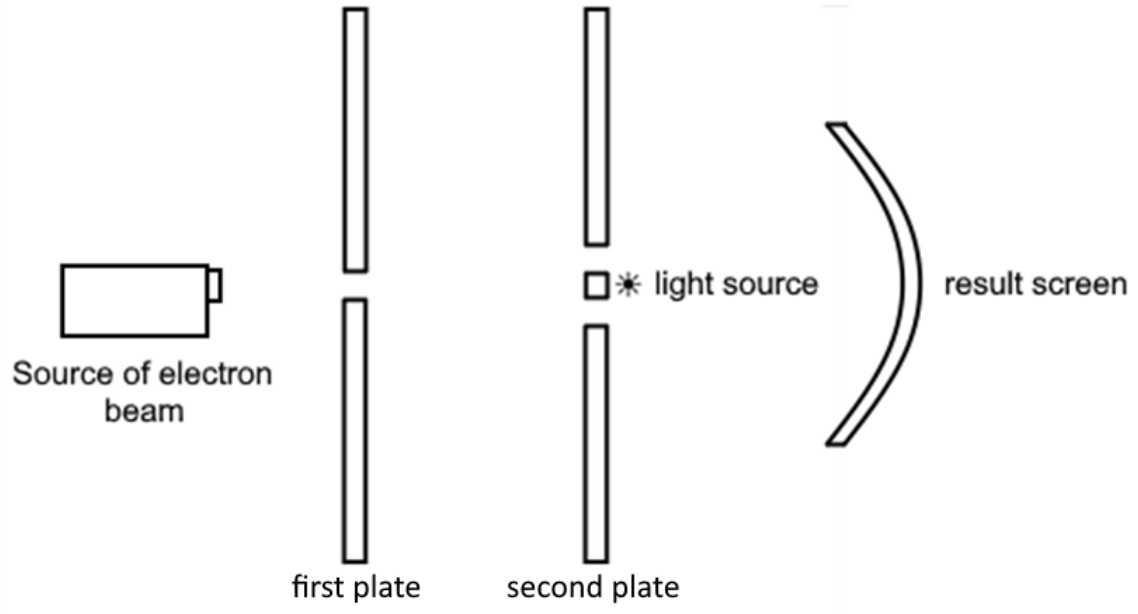

Figure 7: Diagram of the double slit experiment where an electron beam passes through two plates and slits before reaching a screen.

This dilemma is named the uncertainty principle coined by Heisenberg which states that it is not possible to measure a property of a system without influencing complementary variables. In his equation, the momentum p_x and the position x of a particle are approximately the Planck's constant and by accurately measuring one of them it would make the other one less accurate [48,49].

$$\Delta x \Delta p_x \geq \frac{h}{4\pi} \qquad (3)$$

1.2. Schrödinger equation

The culmination of all the prior findings for quantum mechanics came when Erwin Schrödinger postulated his grand equation for physics and chemistry that could describe the coordinates of a particle, for instance x , as a wave function Ψ that would itself be a function of time t.

$$\Psi = \Psi(\mathrm{x},\mathrm{t}) \tag{4}$$

From the concept of wave function and its dependency on time, the time-dependent Schrödinger equation was created:

$$-\frac{\hbar}{i}\frac{\partial\,\Psi(\mathrm{x},\mathrm{t})}{\partial\,t} = -\frac{\hbar^2}{2m}\frac{\partial^2\,\Psi(\mathrm{x},\mathrm{t})}{\partial\,x^2} + \mathrm{V}(\mathrm{x},\mathrm{t})\,\Psi(\mathrm{x},\mathrm{t}) \tag{5}$$

$$\hbar \equiv \frac{h}{2\pi} \tag{6}$$

where the $\hbar$ is the reduced Planck's constant, i is equal to $\sqrt{-1}$, m is the mass of the particle and V is the potential energy function for a one-particle, one-dimensional system.

Fortunately, for most chemistry needs the simpler time-independent Schrödinger equation can be used:

$$E\,\psi(\mathrm{x},\mathrm{t}) = -\frac{\hbar^2}{2m}\frac{d^2\,\psi(\mathrm{x})}{d\,x^2} + \mathrm{V}(\mathrm{x})\,\psi(\mathrm{x}) \tag{7}$$

$$\Psi(\mathrm{x},\mathrm{t}) = f(\mathrm{t})\,\psi(\mathrm{x}) \tag{8}$$

where E is a constant, ψ is the factor of Ψ that depends only on x for a one-particle, one-dimensional system.

Max Born postulated that the $|\Psi(\mathrm{x},\mathrm{t})|^2$ gives the probability density for finding the particle in different regions of the x axis. Thus, the squared wave function is very important for orbital density calculations in chemistry when applying the Schrödinger equation considering three dimensions [48,49].

2. Computational chemistry

The invention and improvements in the field of computer science have allowed chemists to numerically solve the Schrödinger equation for increasingly complex systems composed of multiple electrons and molecules using numerical iteration methods. As a result, it now was possible to model and predict the behavior of atoms, molecules and systems in areas like semiconductors, pharmaceutical and energy storage and many more without the need of expending time and resources in experimental tests [50-52].

However, to reach such methods some approximations had to been applied to facilitate the calculations linked with the Schrödinger equation. Max Born and Julius Robert Oppenheimer simplified the Schrödinger equation by separating the equation in two parts, the first one that describes the electronic wave function for a fixed nuclear geometry and the second one that describes the nuclear wavefunction where the electronic energy plays the role of a potential energy. This approximation is possible because the nuclei are much heavier than electrons and their velocities are also much smaller. Although this approximation created a shortcut from the Schrödinger equation, the sum of electron kinetic energy and the terms regarding the attraction and repulsive potential energies are treated as an average that can lead to inaccuracies in systems with two close electronics states and for elements of the fourth period or higher in the periodic table [53].

Another approximation that came after was the linear combination of atomic orbitals (LCAO) introduced by John Lennard-Jones in 1929 to lower the calculation difficulty. Accomplished by transforming harder exponential functions into gaussian functions, this approach expands the molecular orbitals into a combination of the atomic orbitals of lower computational effort and facilitating the initial guess in the succeeding methods that will be presented [53].

2.1. Hartree-Fock

The Hartree-Fock (HF) is a method that used a series of approximations to solve the Schrödinger equation without requiring experimental data, thus making it an *ab initio* method. Also known as the self-consistent field (SCF) method, it uses a numerical method to calculate the repulsion felt by an electron as the average potential field created

by all the other electrons by means of an iterative process, until it converges into accepting values. Unfortunately, because of the use of average fields, the HF method can give wrong values for the electronic correlation of the repulsion energies.

2.2. Post-Hartree-Fock

Post-HF methods were developed to minimize the inaccuracy of the HF method by calculating the electronic correlation of each orbital instead using the average HF approach. Methods that calculated the correction energy instead provided more accurate representation of systems with higher complexity but would require extra calculations for the higher basis used [53].

2.3. Density functional theory

Density functional theory (DFT) is a computational modelling method created in 1964 by Kohn and Hohenberg [54] to calculate the electronic structure of atoms, molecules and molecular systems. In contrast to traditional methods of trying to resolve Schrödinger equation only using wave functions, DFT as the name implies, utilizes the total electronic density function as the fundamental variable. The *Gaussian 16* program used in this work is capable of simulating the electronic, optical, spectroscopic and many more properties and behaviors of compounds. In this work, it was used to find the ground state geometry and energy levels by making small adjustments in the system geometry and analyzing through DFT calculations how the total electronic density changes until its minimum energy point was found [55].

This analysis is comprised of two key elements: functionals and basis sets. First, the functionals are, in simple terms, the group of functions that are used to calculate the exchange energy and electronic correlation of a quantum system and can be either pure or hybrid functionals. While pure functionals produce results only using electronic density data, hybrid functionals combine pure DFT energy approximations with wave function methods and can use experimental data to increase the accuracy of the results. Basis set are a collection of electron functions centered on atomic nuclei that are used to construct the molecular orbitals of a system with different levels of precision. Sets with more functions produce more accurate results wasting more time but, depending on the

need or system complexity, it is possible to use smaller sets and produce the same results in a shorter period of time [56,57].

In the current project, the MN15 global-hybrid functional was chosen to analyze the capability of 92 molecules in the graphene and graphyne families and their substituents as positive electrodes for LIBs in respect to energy levels, redox potentials and electron affinity. The MN15 method was chosen because it is a new hybrid functional that has shown superior performance over previous functionals in accurately predicting multiple properties. This is particularly crucial in the design of new energy materials and catalysts [58]. Lastly, all calculations used the 6-31+G(d,p) basis set because it provided accurate results in reasonable lengths of time [59-61]. This basis set, called Pople basis set, is comprised of one Slater-type orbital (STO) function for the core electrons with a linear combination of 6 primitives and 2 STOs functions described by 3 primitive Gaussians for the inner part of valence electrons and 1 primitive Gaussian for the outer part of valance electrons. Furthermore, this set uses polarized functions for both heavy and light atoms that account can account for electronic density deformation caused by interactions with other atoms while the non-hydrogen atoms also used diffuse functions to give orbitals more flexibility away from the nucleus.

2.4. Solvation model

In the realm of solution chemistry, it is necessary not only to perform calculations for the object of study but also to understand how the solvent interacts with it and vice versa. This can be done either through an explicit model where the solvent molecules are treated individually together with the main object or through an implicit model where a cavity is created around the main object to electrostatically interact with it. Implicit models basically aim to simulate the interaction that the liquid establish with the main object of study by creating a polarizable surface that require far less computational power in comparison to calculating interactions with each individual solvent molecule [53].

Batteries electrolyte solvents are a subject that has been comprehensively studied because of the specific and constraining conditions that are required in real world applications. One mixture that is widely used is the EC/DMC mixture because EC has a high dielectric constant and degrades into a passive layer that is not prejudicial to the battery while DMC lowers the viscosity and melting point of the mixture [62]. Even though a mixture of EC and DMC with the molar ratio of 3:7 theoretically has the higher ionic

conductivity [63], a mixture containing more EC than DMC has shown to have a more energetically stable electrolyte-solvent complex [64] and a more stable charge and discharge cycle performance [65]. Thus, this project chose an 8:2 molar ratio of EC and DMC to use as the solvent for the solvation free energy calculations.

These energies were calculated using the polarizable continuum model (PCM) with the integrated equation formalism variable (IEFPCM) that creates a solute cavity for the cathode with a set of overlapping spheres that are treated as surface charges [66]. The required PCM inputs for custom solvents are the solvent radius (r), static dielectric constant (ε_s) and dynamic dielectric constant (ε_d), also known as optic dielectric constant.

Due to the lack of empirical data for ε_d and r of the exact mixture used, the ε_d has been approximated [67] to be the square of the mixture's refractive index (n_m) and determined through a series of equations (Eq. 4-7) [68].

$$V_m = \frac{M}{\rho} \tag{9}$$

$$\varphi = \frac{x_i \times v_i}{\sum x_t \times v_t} \tag{10}$$

$$\frac{n_m^2 - 1}{n_m^2 + 2} = \varphi_1 \times \frac{n_1^2 - 1}{n_1^2 + 2} + \varphi_2 \times \frac{n_2^2 - 1}{n_2^2 + 2} \tag{11}$$

$$\varepsilon_d = n_m^2 \tag{12}$$

Initially, the molar volumes (V_m) were calculated using the molar mass (M) and densities (ρ) of EC and DMC [69]. Then, the volume fractions (φ) were determined using the molar volumes and the 8:2 EC/DMC molar fractions of the mixture. The mixture's refractive index was calculated with the volume fractions and the refractive indices of each pure solvent (n_1, n_2) [70,71] and finally the dynamic dielectric constant used in the PCM was determined.

Lastly, the solvent radius parameter was determined [72] from the mixture molecular mass (m), the packing density (Δ_{pd}), and density (ρ) [69].

$$r^3 = \frac{3 \times m \times \Delta_{pd}}{4 \times \pi \times \rho} \times (10^{24}) \tag{13}$$

3. Redox potential

In electrochemical systems, the reduction potentials of the electrodes are not the sole factors that need to be assessed when developing batteries with higher potentials. Thermodynamic and kinetic processes that occur in the electrodes, electrolyte solution and wires can increase resistance and require higher voltage applied to make a reaction happen. Whilst this study will only calculate theoretical reduction potential, it is relevant to mention two factors tied to practical cell reactions and its equilibrium.

The primary aspect is the additional potential over the theoretical value that sometimes is required for a cell reaction to start. Overpotential is caused by a sum of processes that prevents the cell from working, some examples are slow mass transport of reactants in the electrolyte, slow adsorption/desorption of reactants to the electrodes and slow electron transfer between the electrode and reactants [73,74].

Along with overpotential, some extra voltage may be necessary because of the ohmic drops that takes place in the cell and in the circuits. Non-ideal electrode distances, high electrolyte resistance and other resistances present in the system are some of the sources of ohmic drops [75,76]. Although some overpotentials and ohmic drops cannot be eliminated in some cells because they are fundamental in the reactions, most of the time these elements can be reduced with better cell designs and instrumentation [76].

The theoretically standard cell potential for a LIB with an organic cathode is [77,78]:

$$\Delta E^0 = \left(-\frac{\Delta G^{red}(R, sol)}{n_e F} - E_H \right) - E_{Li} \qquad (14)$$

The term E_{Li} refers to the redox potential of the Li/Li$^+$ electrode paired with a standard hydrogen electrode (SHE) that is -3.04 V [79], E_H refers to the absolute redox potential of hydrogen that is 4.44 V [80], n_e represents the number of electrons involved in the reaction while *F* represents the Faraday constant and $\Delta G^{red}(R, sol)$ is the energy required to reduce the cathode in a solution.

However, it has been proven that direct DFT calculations of the two immediate states of this free energy leads to inaccurate results [78]. In a way to circumvent this issue [77,78,81], the $\Delta G^{red}(S, sol)$ was determined by using the thermodynamic cycle (Fig. 8) in the following equation:

$$\Delta G^{red}(R, sol) = \Delta G^{red}(R, gas) + \Delta G^{solv}(R^-) - \Delta G^{solv}(R) \qquad (15)$$

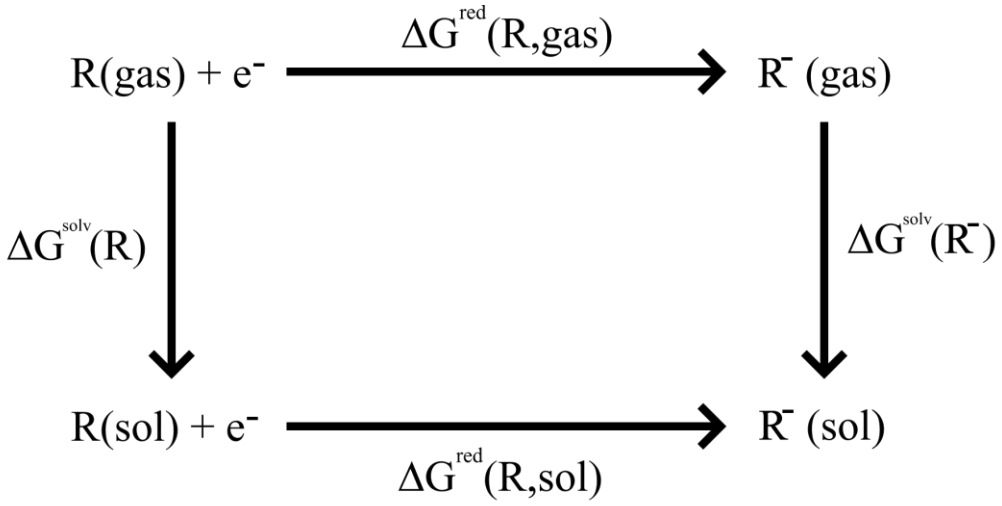

Figure 8: Diagram of the thermodynamic cycle adopted to calculate the free energy of the reduction in solution of cathodes.

Accordingly, $\Delta G^{red}(R, gas)$ is the Gibbs free energy of the reduction in a gas phase, $\Delta G^{solv}(R^-)$ is the Gibbs free energy of solvation in an anionic state and $\Delta G^{solv}(R)$ is the Gibbs free energy of solvation in a neutral state.

4. Correlation analysis

It has been already noted [22,82] a strong linear relation between electron affinity and its redox potential; hence this work has screened a large group of different carbon nanomaterials with substituents and correlated their electron affinity to estimate the redox and compare to the calculated redox potentials using the thermodynamic cycle. Electron affinity can be defined as the amount energy released when a molecule or atom in gaseous phase and in its electronic ground state receives an electron.

MN15 functional was chosen to survey the electron affinity of a wide range of molecules and identify promising candidates as LIB electrodes because it provides the best results for single-reference systems [83].

Chapter III

Results and Discussion

1. Redox potential

In this study, the redox potentials of pristine and edge-substituted graphene and graphyne were investigated for their application as electrodes in LIBs. The structures of $C_{54}H_{18}$ graphene and $C_{66}H_{18}$ graphyne sheets were modeled, optimized at the MN15/6-31+G(d,p) level of accuracy without any geometry constraints and used as the blueprint for all substituted compounds in this project (Fig. 9). Graphene systems were modeled from a base graphene structure comprised of 54 carbon atoms because it reliably represents the properties of larger graphene sheets without requiring long computational times [84]. Graphyne systems, on the other hand, were modeled from a base graphyne structure comprised of 66 carbon atoms because of the symmetrical and size similarities to the base graphene structure. A total of twelve substituents were studied in this project being the carbonyl (-O), fluoride (-F), chloride (-Cl), hydroxyl (-OH), amino ($-NH_2$), nitrile (-CN), nitro ($-NO_2$), carboxyl (-COOH), trichloromethyl ($-CCl_3$), trifluoromethyl ($-CF_3$), sulfeno (-SOH) and dimethylamino ($-N(CH_3)_2$) groups.

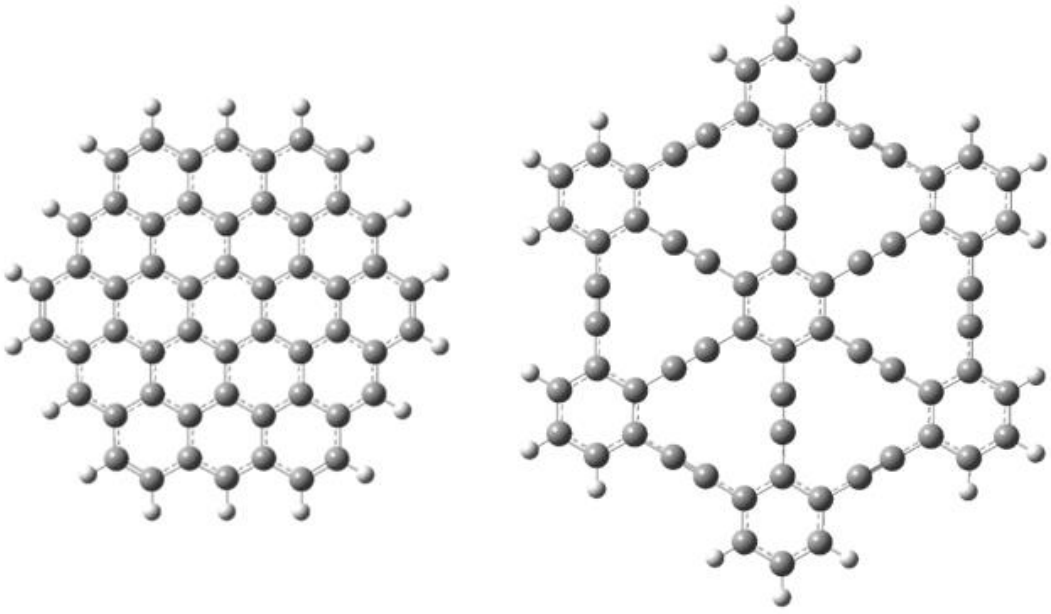

Figure 9: Structures of pristine graphene (left) and pristine graphyne (right) used in this work.

The first set of compounds comprised of 29 graphenes and 15 graphynes that explored seven groups for the graphene being the carbonyl, fluoride, chloride, hydroxyl, amino, nitrile, nitro groups and three for the graphyne being the carbonyl, hydroxyl and nitro

groups that were modeled to account for different positional isomers in three different types of configurations. When the substituents were place opposed, intercalated or close to each other. In the opposed configuration substituents are symmetrically opposed from one another, in the intercalated configuration substituents have one carbon between the substituted carbons and in the close configuration the substituted carbons are adjacent to each other (Fig. 10). In some of these configurations there were also modeled positional isomers to see if would affect the redox potential.

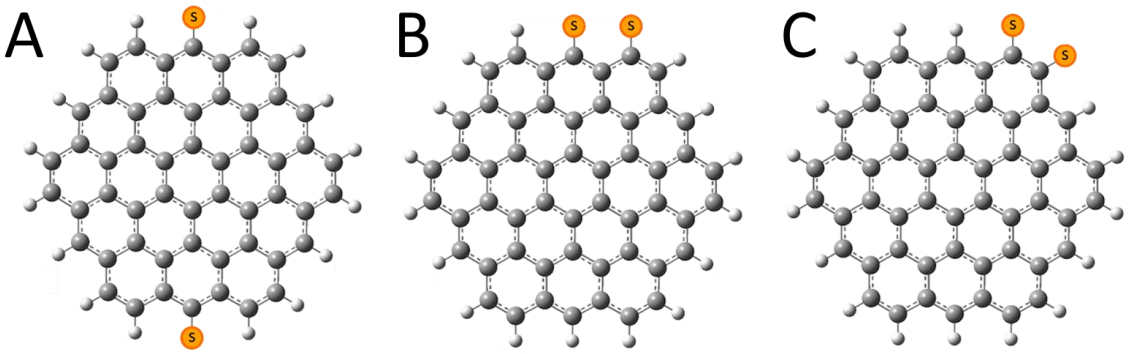

Figure 10: Representation of the three configurations in the first set; (A) opposed, (B) intercalated and (C) close.

The second set of compounds comprised of 56 graphynes that explored eight groups being the carbonyl, nitrile, nitro, carboxyl, trichloromethyl, trifluoromethyl, sulfeno and dimethylamino groups were modeled to account for different positional isomers in two different configurations. In the first configuration the substituents were continuously added locally in the framework and in the second configuration they were continuously added uniformly in the graphyne.

It is important to mention that the pristine graphyne and 8 substituted graphynes with carbonyl and nitro groups will appear in both Tables to allow for comparison inside each set but they are in fact the same molecule. The 8 substituted compounds are repeated because the different configuration methods in each set reached the same final geometry of these specific compounds.

Lastly, the parameters required for the PCM computation using the 8:2 molar ratio mixture of EC and DMC were 62.43 for the static dielectric constant [85], 1.380 for the dynamic dielectric constant and 2.41 Å for solvent radius. These two last parameters were calculated through a series of formulas mentioned in the solvation model section in the methodology chapter (Appendix 1).

1.1. Opposed, intercalated and close compounds

The redox potential and electron affinity for 29 compounds based on graphene and 15 compounds based on graphyne are depicted Table 1 and Table 2 respectively. The numbering scheme for graphene and graphyne is illustrated in Figure 11 and Figure 12 respectively. This scheme was employed to help visualize and identify the specific sites of functionalization that are given in parenthesis in each Table.

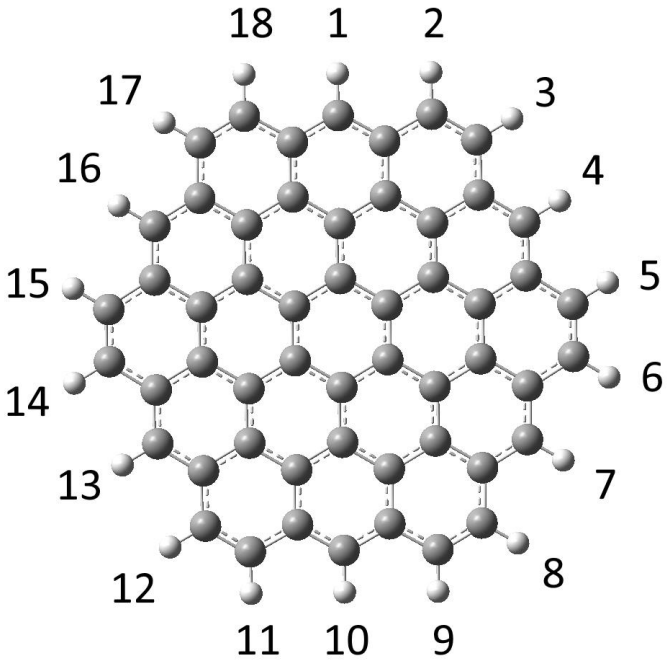

Figure 11: Diagram of the graphene structure with the substituent sites enumerated.

When compared to the 1.4 V redox potential of the pristine graphene, the only monosubstituted graphenes with particularly higher potential are those corresponding to the nitrile, nitro or carbonyl groups with the redox potential of 1.8, 2.1 and 2.9 V, respectively.

The dominance of the hydroxyl group over the carbonyl group as an oxygen functional group in synthesized graphene oxides may be attributed to the comparatively higher stability of the hydroxyl group [86]. Consequently, monosubstituted graphenes were later modeled with the addiction of one hydroxyl group to examine the effect on the redox potentials of product-derived compounds after a hydroxylation reaction occurs.

Compounds Ge9 to Ge12 show no change in redox potential when the monosubstituted graphenes are further substituted with a hydroxy group. In contrast, the Ge10 molecule exhibits a significant reduction in redox potential, decreasing the value to 1.4 V compared to 1.8 V of compound Ge4. Additionally, Ge13 to Ge16 structural isomers of the Ge12 compound were modeled to account for possible combinations when both groups are *close* to each other in the molecule but at different configurations. The results, in particular of the Ge13 molecule, show that hydroxylation of these monosubstituted compounds can lead to an increase in the redox potential of the electrode if the control of the substitution position is possible.

Table 1

Redox potential and electron affinity of graphene compounds of the first set with information of their substituents and the respective position between parentheses.

Identifier	R1	R2	R3	R4	Redox potential (V vs. Li/Li+)	Electron affinity (eV)
Pristine						
Ge1	-	-	-	-	1.4	-1.38
Monosubstituted						
Ge2	F (1)	-	-	-	1.5	-1.46
Ge3	Cl (1)	-	-	-	1.5	-1.47
Ge4	CN (1)	-	-	-	1.8	-1.80
Ge5	NH_2 (1)	-	-	-	1.4	-1.23
Ge6	O (1)	-	-	-	2.9	-2.88
Ge7	OH (1)	-	-	-	1.4	-1.39
Ge8	NO_2 (1)	-	-	-	2.1	-1.90
Disubstituted with hydroxyl group						
Ge9	F (1)	OH (2)	-	-	1.5	-1.48
Ge10	CN (1)	OH (2)	-	-	1.4	-1.75
Ge11	NH_2 (1)	OH (2)	-	-	1.4	-1.36
Ge12	NO_2 (1)	OH (10)	-	-	2.1	-1.87
Ge13	NO_2 (2)	OH (1)	-	-	2.6	-2.31
Ge14	NO_2 (2)	OH (3)	-	-	2.3	-2.04
Ge15	NO_2 (2)	OH (18)	-	-	2.3	-1.92
Ge16	NO_2 (2)	OH (4)	-	-	2.2	-1.91
Multi-substituted						
Ge17	O (2)	O (3)	-	-	2.6	-2.26
Ge18	O (1)	O (2)	-	-	3.1	-3.27
Ge19	O (2)	O (3)	O (4)	-	3.5	-3.44
Ge20	O (1)	O (2)	O (3)	O (18)	3.7	-3.81
Ge21	O (1)	O (2)	O (3)	O (4)	3.8	-2.60
Ge22	NO_2 (1)	NO_2 (10)	-	-	1.6	-1.85
Ge23	NO_2 (2)	NO_2 (18)	-	-	2.3	-2.17
Ge24	NO_2 (1)	NO_2 (3)	NO_2 (17)	-	2.1	-2.60
Ge25	NO_2 (1)	NO_2 (7)	NO_2 (13)	-	2.2	-2.34
Ge26	NO_2 (1)	NO_2 (5)	NO_2 (10)	NO_2 (14)	2.3	-2.70
Ge27	NO_2 (2)	NO_2 (4)	NO_2 (16)	NO_2 (18)	2.6	-2.66
Ge28	F (1)	F (2)	F (3)	F (18)	1.6	-1.72
Ge29	CN (1)	CN (2)	CN (3)	CN (18)	2.4	-5.57

In the multi-substituted branch of compounds, the process of adding more substituents generally increases the value of the redox potential of most compounds like in the case of the carbonyl compounds, Ge17 to Ge21, and nitro compounds, Ge22 to Ge27. When the compounds had their substituent groups spaced apart instead of clumped together in one side of the molecule, a lower redox potential has been displayed. The only exception to this pattern happens in the case of the trinitrographene Ge24 and Ge25 isomers, where the non-symmetrical isomer has a slightly lower redox potential. In the case of the graphene with four fluoride substituents, Ge28, a slightly increase in the value of the redox potential makes the continuous addition of substituents not worth it to be further explored, likewise the chloride group was skipped because similar results were expected based on their chemical properties.

The nitro and carbonyl groups were chosen as the substituents to be studied in the graphyne system due to their high performance observed in graphene. Hence, the data obtained for Gy2 to Gy4 compounds demonstrate similar trends to their analogous counterparts in the graphene system. Specifically, the nitro and carbonyl compounds exhibit a significant increase in redox potential, while the hydroxyl compound demonstrates the same redox potential as their pristine counterpart. The disubstituted carbonyl-graphyne Gy7 and the disubstituted nitrographyne Gy13 exhibit higher potential than the corresponding graphene cases, namely 4.1 V and 2.8 V, respectively. However, increasing the number of substituents does not result in higher redox potential of the compound like in the graphene system.

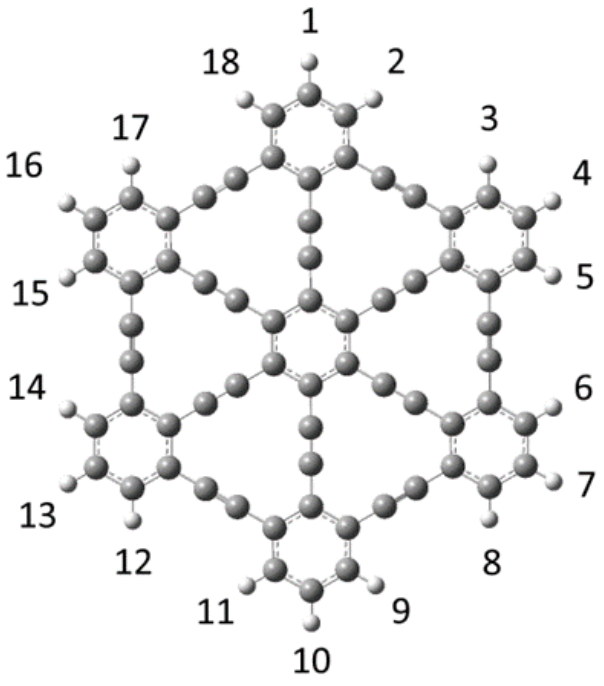

Figure 12: Diagram of the graphyne structure with the substituent sites enumerated.

Table 2

Redox potential and electron affinity of the graphyne compounds of the first set with information of their substituents and the respective position between parentheses.

Identifier	R1	R2	R3	R4	Redox potential (V vs. Li/Li+)	Electron affinity (eV)
Pristine						
Gy1	-	-	-	-	2.1	-1.89
Monosubstituted						
Gy2	OH (1)	-	-	-	2.1	-1.91
Gy3	O (1)	-	-	-	3.5	-3.23
Gy4	NO_2 (1)	-	-	-	2.5	-2.36
Multi-substituted						
Gy5	O (1)	O (2)	-	-	3.3	-3.01
Gy6	O (1)	O (10)	-	-	3.8	-3.97
Gy7	O (2)	O (18)	-	-	4.1	-3.87
Gy8	O (1)	O (7)	O (13)	-	2.7	-2.91
Gy9	O (1)	O (2)	O (18)	-	3.7	-3.58
Gy10	NO_2 (2)	NO_2 (3)	-	-	2.5	-2.25
Gy11	NO_2 (1)	NO_2 (3)	-	-	2.5	-2.49
Gy12	NO_2 (1)	NO_2 (10)	-	-	2.6	-2.65
Gy13	NO_2 (2)	NO_2 (18)	-	-	2.8	-2.59
Gy14	NO_2 (1)	NO_2 (7)	NO_2 (13)	-	2.3	-2.74
Gy15	NO_2 (2)	NO_2 (3)	NO_2 (17)	NO_2 (18)	2.8	-2.78

1.2. Uniform and local compounds

The redox potential and electron affinity for 57 compounds based on graphyne are split into Table 3 and Table 4. The methodology of how each substituent was placed into the graphyne lattice is depicted in Figure 13 resulting in seven different compounds for each type of substituent group from monosubstituted into the multi-substituted in both uniform and local configurations. Unfortunately, data for Gy34, Gy47 and Gy53 in some of their points in the thermodynamic cycle did not finish in time for the publication of this work, therefore it was not possible to calculate their redox potentials. Furthermore, only the Gy47 had the necessary points to calculate their electron affinity. As mentioned before, compounds Gy23*, Gy24*, Gy25*, Gy27*, Gy65*, Gy66*, Gy67* and Gy69* already were presented in the previous section as compounds Gy4, Gy12, Gy14, Gy13, Gy3, Gy6,

Gy8 and Gy7 respectively and have an asterisk in their entries in Table 3 and Table 4 to ensure that they are not represented as new data.

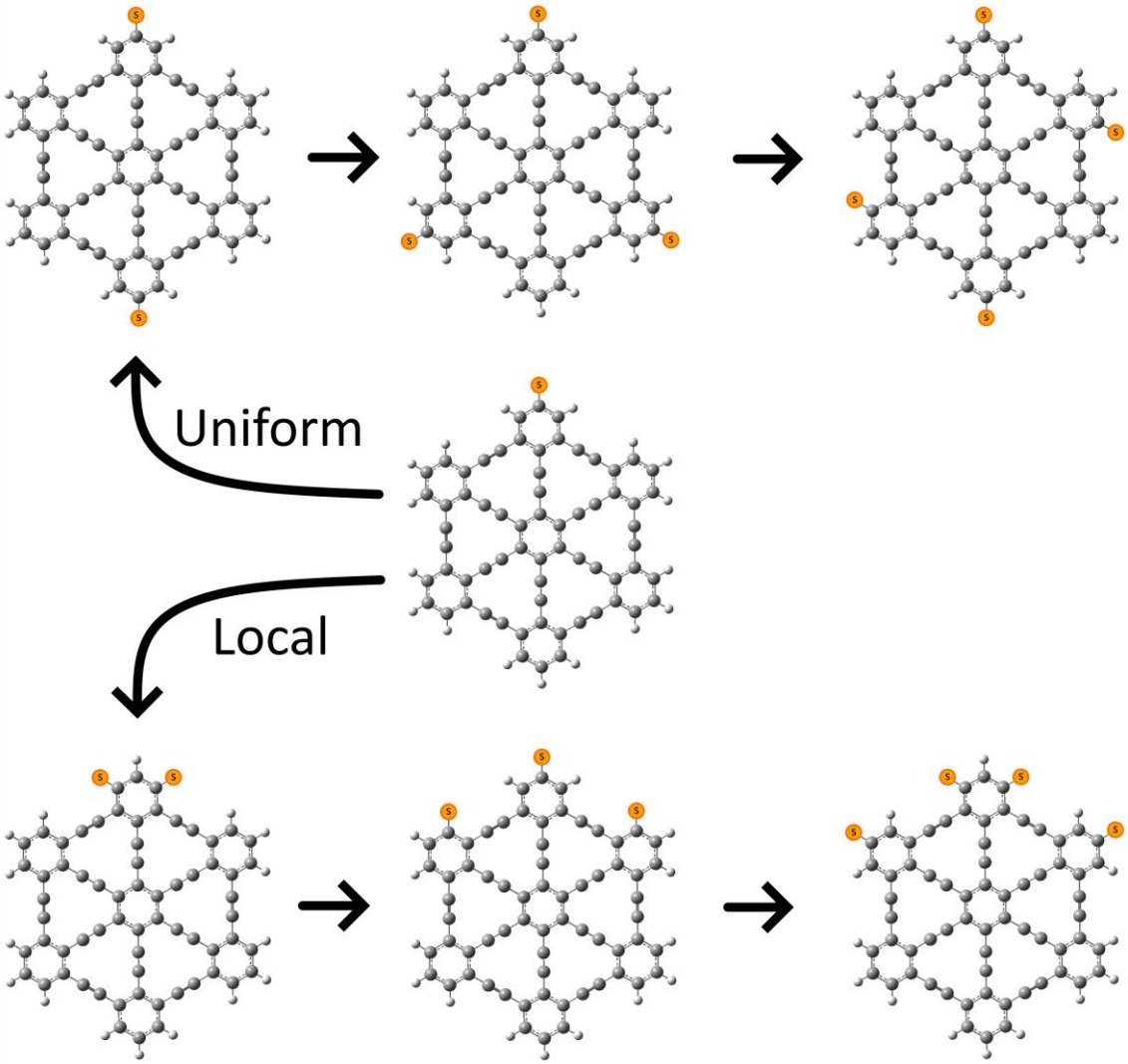

Figure 13: Substitution methodology for the second set of compounds where the substituent sites are indicated by an orange color.

Taking the redox potential of pristine graphyne, 2.1 V, as comparison, the only monosubstituted compounds that present notable increases are those with the nitro and carbonyl groups Gy23* and Gy65* with 2.5 V and 3.5 V respectively. Unlike the trend in graphene where three groups being these two groups and nitrile group showed the same increased relative potential, in the graphyne system the monosubstituted nitrilegraphyne showed no noticeable increase in redox potential of only 2.2 V. This divergence continued when further substitutions were done with more nitrile groups when the

graphene system showed a very big increase in redox potential while the graphyne system showed no markable increase in both configurations of Gy33 and Gy36 with the same redox potential of 2.4 V.

In fact, the only substituents in graphyne that showed any noteworthy increases in redox potential at their multi-substituted compounds were the nitro, carbonyl and trifluoromethyl. Thus, these three substituents will be further analyzed since the other four showed no valuable increase in the redox potential, in particular the Gy60 with three dimethylamino groups in the uniform configuration that showed a decrease in redox potential to 1.9 V compared to the pristine state, that being the lowest of all graphynes studied.

Similar to the graphene, the continuous addition of nitro and carbonyl groups in the graphyne system showed higher redox potentials reaching 2.9 V and 5.0 V for their respective four local substituted graphynes Gy29 and Gy71. In both of their multi-substituted compounds, the positional isomers in the local configuration Gy28, Gy29, Gy69*, Gy70 and Gy71 showed higher redox potential when compared to their uniform configuration counterparts Gy25*, Gy26*, Gy66*, Gy67* and Gy68. The exception to this trend was the uniformly disubstituted nitrographyne Gy24* that showed a higher redox potential of 2.6 V while their local counterpart Gy27* had lower redox potential when compared to the redox state of 2.0 V.

One evident point seen in the multi-substituted carbonyl-graphynes is the fact that compounds with odd number of substituents show lower increases in the redox potential when compared to the graphynes with an even number of substituents. This behavior is likely due to the fact that odd number of substituents are doublets while graphynes with even number of substituents are singlets.

Lastly, the only substituent that did not follow the overall trend of their family was the tetrasubstituted trifluoromethyl-graphyne in the local configuration Gy50 that aside from nitro and carbonyl graphynes showed a notable increase in the redox potential to 2.9 V. Sadly, their uniform counterpart Gy47 was one of the compounds that has no redox potential data but it has the electron affinity data allowing to predict its redox potential. Using the redox potential correlation that will be showed in the next sections, it is possible to predict that its redox potential would be 2.5 V. Although it is a small increase in redox potential, is half of the increase shown by compound Gy50.

Table 3

Redox potential and electron affinity of the first half of graphyne compounds of the second set.

Identifier	Compound	Redox potential (V vs. Li/Li+)	Electron affinity (eV)
Pristine			
Gy1	No substituents	2.1	-1.89
Carboxyl substituted compounds (-COOH)			
Gy16	Monosubstituted	2.2	-2.28
Gy17	2 Uniformly distributed groups	2.3	-2.28
Gy18	3 Uniformly distributed groups	2.2	-2.46
Gy19	4 Uniformly distributed groups	2.3	-2.10
Gy20	2 Locally distributed groups	2.2	-2.10
Gy21	3 Locally distributed groups	2.2	-2.27
Gy22	4 Locally distributed groups	2.2	-2.39
Nitro substituted compounds (-NO_2)			
Gy23 *	Monosubstituted	2.5	-2.36
Gy24 *	2 Uniformly distributed groups	2.6	-2.65
Gy25 *	3 Uniformly distributed groups	2.3	-2.74
Gy26	4 Uniformly distributed groups	2.6	-2.98
Gy27 *	2 Locally distributed groups	2.0	-2.59
Gy28	3 Locally distributed groups	2.6	-2.62
Gy29	4 Locally distributed groups	2.9	-2.98
Nitrile substituted compounds (-CN)			
Gy30	Monosubstituted	2.2	-2.20
Gy31	2 Uniformly distributed groups	2.3	-2.45
Gy32	3 Uniformly distributed groups	2.3	-2.55
Gy33	4 Uniformly distributed groups	2.4	-2.75
Gy34	2 Locally distributed groups	-	-
Gy35	3 Locally distributed groups	2.3	-2.48
Gy36	4 Locally distributed groups	2.4	-2.71
Sulfeno substituted compounds (-SOH)			
Gy37	Monosubstituted	2.1	-2.26
Gy38	2 Uniformly distributed groups	2.1	-2.09
Gy39	3 Uniformly distributed groups	2.1	-2.08
Gy40	4 Uniformly distributed groups	2.1	-2.13
Gy41	2 Locally distributed groups	2.1	-1.98
Gy42	3 Locally distributed groups	2.1	-2.09
Gy43	4 Locally distributed groups	2.1	-2.08

Table 4

Redox potential and electron affinity of the second half of graphyne compounds of the second set.

Identifier	Compound	Redox potential (V vs. Li/Li+)	Electron affinity (eV)
Pristine			
Gy1	No substituents	2.1	-1.89
Trifluoromethyl substituted compounds (-CF_3)			
Gy44	Monosubstituted	2.2	-2.02
Gy45	2 Uniformly distributed groups	2.2	-2.28
Gy46	3 Uniformly distributed groups	2.4	-2.36
Gy47	4 Uniformly distributed groups	-	-2.52
Gy48	2 Locally distributed groups	2.2	-2.11
Gy49	3 Locally distributed groups	2.3	-2.30
Gy50	4 Locally distributed groups	2.9	-2.44
Trichloromethyl substituted compounds (-CCl_3)			
Gy51	Monosubstituted	2.2	-2.10
Gy52	2 Uniformly distributed groups	2.2	-2.25
Gy53	3 Uniformly distributed groups	-	-
Gy54	4 Uniformly distributed groups	2.3	-2.48
Gy55	2 Locally distributed groups	2.2	-2.11
Gy56	3 Locally distributed groups	2.2	-2.29
Gy57	4 Locally distributed groups	2.3	-2.40
Dimethylamino substituted compounds (-$N(CH_3)_2$)			
Gy58	Monosubstituted	2.1	-1.80
Gy59	2 Uniformly distributed groups	2.0	-1.71
Gy60	3 Uniformly distributed groups	1.9	-1.50
Gy61	4 Uniformly distributed groups	2.0	-1.61
Gy62	2 Locally distributed groups	2.1	-1.91
Gy63	3 Locally distributed groups	2.2	-1.81
Gy64	4 Locally distributed groups	2.0	-1.69
Carbonyl substituted compounds (-O)			
Gy65 *	Monosubstituted	3.5	-3.23
Gy66 *	2 Uniformly distributed groups	3.8	-3.97
Gy67 *	3 Uniformly distributed groups	2.7	-2.91
Gy68	4 Uniformly distributed groups	4.8	-5.38
Gy69 *	2 Locally distributed groups	4.1	-3.87
Gy70	3 Locally distributed groups	2.9	-2.90
Gy71	4 Locally distributed groups	5.0	-5.23

2. Surface charge distribution

Electron distribution has been computed to analyze the impact of functionalization on the surface charges of graphyne framework. Compounds Gy26, Gy39, Gy60 and Gy68 were chosen to be presented as illustrative examples because they show some of the highest and lowest redox potentials (Fig. 14). All other substituted graphynes surface charge calculations were also performed (Appendix 2).

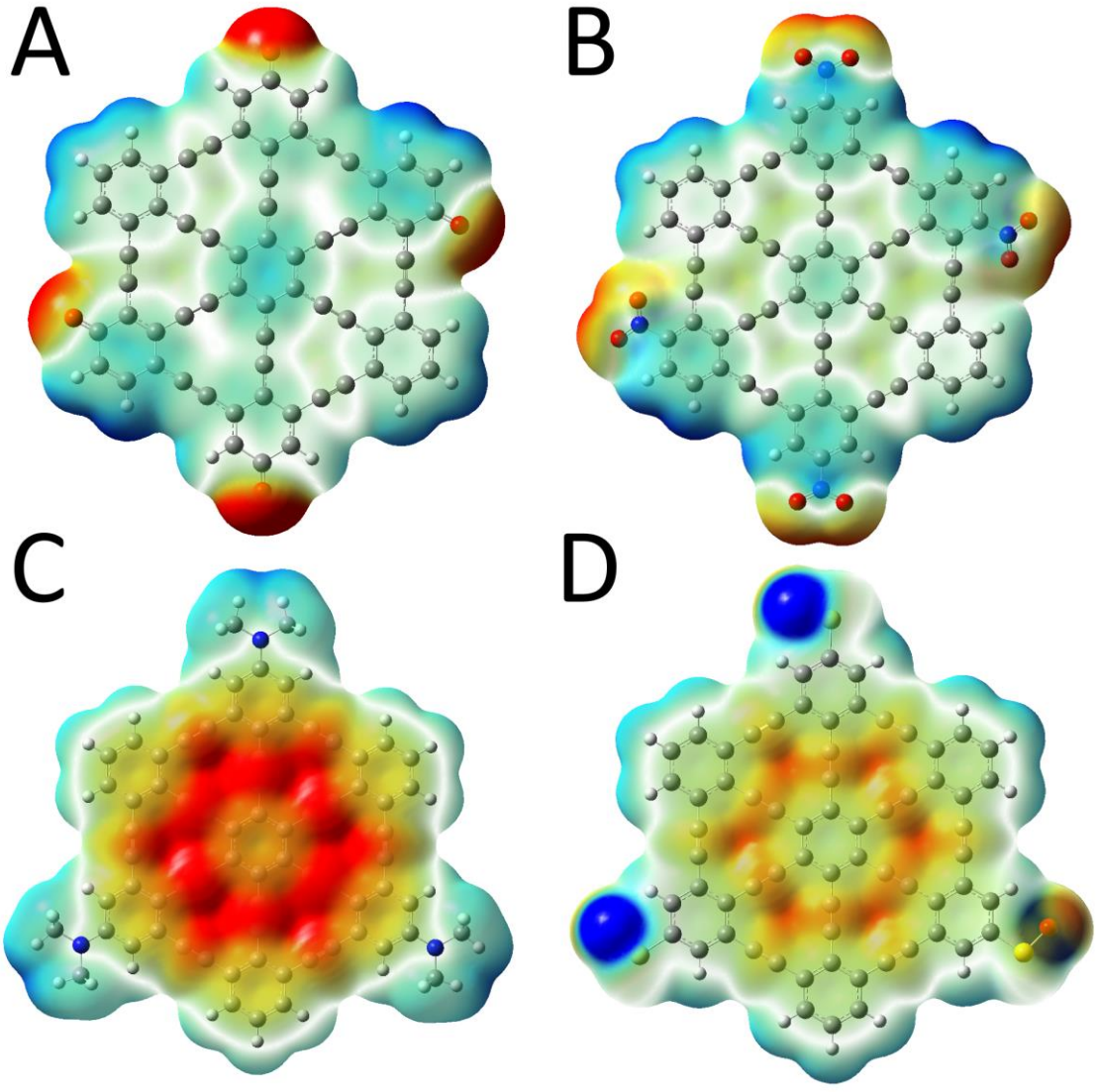

Figure 14: Close-up of Gy68 (A), Gy26 (B), Gy60 (C) and Gy39 (D) compounds. Atoms represented are carbon (grey), hydrogen (white), nitrogen (blue), oxygen (red) and sulfur (yellow).

Surface charge values shown range from -0.4 to +0.4 atomic units (a.u.) where red is associated with negative values and blue is associated with positive values. Compounds A and B with some the highest redox potentials of 4.8 V and 2.6V respectively show high

negative values in their substituents and a very well distributed charge in the carbon framework without any concentration of positive or negative charge. On the contrary, compounds C and D with lowest redox potentials of 1.9 V and 2.1 V show substituents without isolated negative partial charges and show that the carbon framework charge distributions contain high values of negative charge that impact the ability of the compounds to absorb electrons and consequently store lithium-ions.

3. Correlation analysis

Lastly, from the compounds electronic properties it was possible to analyze the linear correlation that exist between redox potential and electronic affinity that was mentioned before. The gathered data from the compounds depicted in Table 1, Table 2, Table 3 and Table 4 was used to create the graph shown in Figure 15 that has two linear correlations with coefficients 0.4497 and 0.8997 for graphene and graphyne systems, respectively. The lower value of the former is justified by the facts that graphene sample size is less than half of graphyne's and the presence of two outliers corresponding to the tetracyanographene and the tetracarbonyl-graphene that if ignored would turn the linear correlation coefficient for graphene system to 0.8849.

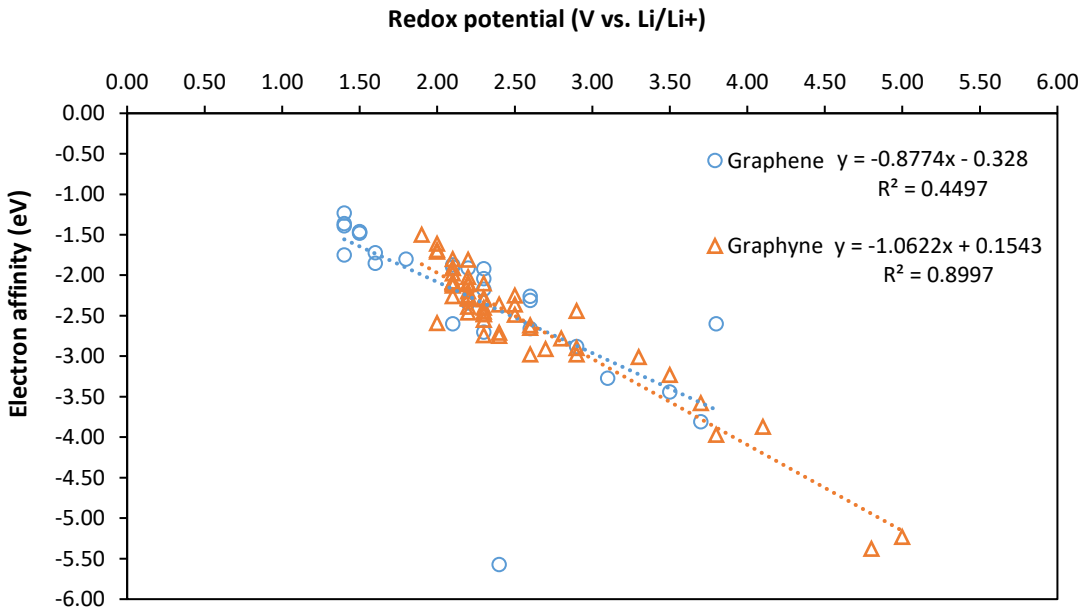

Figure 15: Linear correlation between redox potential and electron affinity in the graphene (blue circles) and graphyne (orange triangles) compounds.

The correlation can be explained by the fact that electron affinity is the energy released when one electron is captured by the neutral substance in the gas phase to form the corresponding anion. This property plays a crucial role in the estimation of the redox potential from the thermodynamic cycle (Fig. 8). This strategy to predict redox potential saves in most cases half of the computation time required to produce the redox potential data.

Chapter IV

Conclusion

In summary, this work provides the redox potential data for pristine and 90 edge mono- or multi-substituted graphenes and graphynes calculated at the DFT/MN15/6-31+G(d,p) level of theory for implementation in LIBs. Graphene data shows that introducing nitro, carbonyl or nitrile groups into the graphene notably increases the redox potential of the compound with only one addition and it keeps rising with further substitutions. By contrast, other substituents did not impact the redox potential when compared to the pristine state even with further substitutions as in the case of tetrafluorographene. Graphyne data reveals that the functionalization of graphyne with carbonyl and nitro groups were the only ones to assure an enhance in the redox potential up to 5.0 V and 2.9 V, respectively, suggesting that this material is a good candidate for lithium-ion batteries with higher potential needs. While one of the multi-substituted trifluoromethyl graphynes matched the nitro group with a potential of 2.9 V, the rest of their family did not show any significant increase in redox potential making it a hard pick because of the very specific number and position of substituents needed. Surface charge analysis reveals the impact of the substituents groups in the graphyne system. Results show that compounds with higher redox potential have well distributed partial charges in the carbon structure while the substituents hold most of the negative partial charges. Additionally, this study ends by highlighting the noteworthy linear correlations between the redox potentials of the compounds investigated and their electronic properties, including electron affinities. This finding presents an opportunity to employ a methodological approach, which provides valuable guiding information derived from an extensive range of potential substituents, requiring less computational time prior to conducting more precise calculations.

List of References

[1] de Santillana, G. (1965). Alessandro Volta. *Scientific American*, *212*(1), 82-91.
[2] Mertens, J. (1998). From the lecture room to the workshop: John Frederic Daniell, the constant battery and electrometallurgy around 1840. *Annals of Science*, *55*(3), 241-261.
[3] Pavlov, D. (2011). *Lead-acid batteries: Science and Technology: A handbook of lead-acid battery technology and its influence on the product*. Elsevier Science Ltd.
[4] Jung, J., Zhang, L., & Zhang, J. (2016). *Lead-acid battery technologies: Fundamentals, materials, and applications.* CRC Press.
[5] Straits Research. (2024, January), *Lead Acid Battery Market Size, Share & Trends Analysis Report By Product (SLI, Motive, Stationary), By Construction Method (Flooded, Valve Regulated Sealed Lead–acid battery (VRLA)), By Applications (Automotive, UPS, Telecom, Others) and By Region(North America, Europe, APAC, Middle East and Africa, LATAM) Forecasts, 2023-2031*, Straits Research https://straitsresearch.com/report/lead-acid-battery-market, Accessed 29 August 2024.
[6] Fichtner, M., Edström, K., Ayerbe, E., Berecibar, M., Bhowmik, A., Castelli, I. E., Clark, S., Dominko, R., Erakca, M., Franco, A. A., Grimaud, A., Horstmann, B., Latz, A., Lorrmann, H., Meeus, M., Narayan, R., Pammer, F., Ruhland, J., Stein, H., Vegge, T., Weil, M. (2022). Rechargeable Batteries of the Future—The State of the Art from a BATTERY 2030+ Perspective. *Advanced Energy Materials*, *12*(17), 2102904.
[7] Chakkaravarthy, C., Periasamy, P., Jegannathan, S., & Vasu, K. I. (1991). The nickel/iron battery. *Journal of Power Sources*, *35*(1), 21-35.
[8] Tsais, P. J., & Chan, L. I. (2013). 11 - Nickel-based batteries: materials and chemistry. In Z. Melhem (Ed.), *Electricity Transmission, Distribution and Storage Systems* (pp. 309-397). Woodhead Publishing.
[9] Liu, W., Placke, T., & Chau, K. T. (2022). Overview of batteries and battery management for electric vehicles. *Energy Reports*, *8*, 4058-4084.
[10] Wang, L., Wang, J., Wang, L., Zhang, M., Wang, R., & Zhan, C. (2022). A critical review on nickel-based cathodes in rechargeable batteries. *International Journal of Minerals, Metallurgy and Materials*, *29*(5), 925-941.
[11] Liu, B., Liu, X., Fan, X., Ding, J., Hu, W., & Zhong, C. (2020). 120 Years of nickel-based cathodes for alkaline batteries. *Journal of Alloys and Compounds*, *834*, 155185.
[12] El Idi, M. M., Karkri, M., & Abdou Tankari, M. (2023). Chapter 14 - Passive thermal management systems for e-mobility using PCM composites. In F. Aloui, E. G. Varuvel, & A. Sonthalia (Eds.), *Handbook of Thermal Management Systems* (pp. 323-369). Elsevier.
[13] Nishi, Y. (2001). Lithium ion secondary batteries; past 10 years and the future. *Journal of Power Sources*, *100*(1), 101-106.
[14] Peng, C., Kong, L., Li, Y., Fu, H., Sun, L., Feng, Y., & Feng, W. (2021). Fluorinated graphene nanoribbons from unzipped single-walled carbon nanotubes for ultrahigh energy density lithium-fluorinated carbon batteries. *Science China Materials, 64*(6), 1367-1377.
[15] Zhang, T., Li, Z., Hou, W., & Yang, Y. (2020). Nanomaterials for implantable batteries to power cardiac devices. *Materials Today Nano, 9*, 100070.
[16] Krause, F. C., Jones, J.-P., Jones, S. C., Pasalic, J., Billings, K. J., West, W. C., Smart, M. C., Bugga, R. V., Brandon, E. J., & Destephen, M. (2018). High Specific Energy Lithium Primary Batteries as Power Sources for Deep Space Exploration. *Journal of The Electrochemical Society, 165*(10), A2312-A2320.
[17] Ramanan, A. (2019). Nobel Prize in Chemistry 2019. *Resonance*, *24*(12), 1381-1395.
[18] Armand, M., & Tarascon, J. M. (2008). Building better batteries. *Nature*, *451*(7179), 652-657.

[19] Markets and Markets. (2023, August), *Lithium-ion Battery Market Size, Share, Statistics and Industry Growth Analysis Report by Type (NMC, LFP, LCO, LTO, LMO, NCA), Capacity (Below 3,000 mAh, 3,001 mAh-10,000 mAh, 10,001 mAh-60,000 mAh, Above 60,000 mAh), Voltage (Below 12V, 12V-36V, Above 36V), Application and Region Global Forecast to 2032*, Markets and Markets https://www.marketsandmarkets.com/Market-Reports/lithium-ion-battery-market-49714593.html, Accessed 29 August 2024.
[20] Sun, C., Feng, Y., Li, Y., Qin, C., Zhang, Q., & Feng, W. (2014). Solvothermally exfoliated fluorographene for high-performance lithium primary batteries. *Nanoscale, 6*(5), 2634-2641.
[21] Contreras, C. N., Cocoletzi, H. H., & Anota, E. C. (2011). Theoretical study of the electronic properties of fluorographene. *Journal of Molecular Modeling, 17*(8), 2093-2097.
[22] Zhu, Y., Kim, K. C., & Jang, S. S. (2018). Boron-doped coronenes with high redox potential for organic positive electrodes in lithium-ion batteries: a first-principles density functional theory modeling study. *Journal of Materials Chemistry A, 6*(21), 10111-10120.
[23] Mutoh, M., Abe, S., Kusaka, T., Nakamura, M., Yoshida, Y., Iida, J., & Tachikawa, H. (2016). Density Functional Theory (DFT) Study on the Ternary Interaction System of the Fluorinated Ethylene Carbonate, Li+ and Graphene Model. *Atoms, 4*(1).
[24] Diederichsen, K. M., & McCloskey, B. D. (2020). Electrolyte additives to enable nonaqueous polyelectrolyte solutions for lithium ion batteries. *Molecular Systems Design & Engineering, 5*(1), 91-96.
[25] Lee, S., & Park, S. S. (2012). Thermodynamic and dynamic properties in binary mixtures of propylene carbonate with dimethyl carbonate and ethylene carbonate. *Journal of Molecular Liquids, 175*, 97-102.
[26] Barnes, T. A., Kaminski, J. W., Borodin, O., & Miller, T. F. (2015). Ab Initio Characterization of the Electrochemical Stability and Solvation Properties of Condensed-Phase Ethylene Carbonate and Dimethyl Carbonate Mixtures. *The Journal of Physical Chemistry C, 119*(8), 3865-3880.
[27] Hassoun, J., Bonaccorso, F., Agostini, M., Angelucci, M., Betti, M. G., Cingolani, R., Gemmi, M., Mariani, C., Panero, S., Pellegrini, V., & Scrosati, B. (2014). An Advanced Lithium-Ion Battery Based on a Graphene Anode and a Lithium Iron Phosphate Cathode. *Nano Letters, 14*(8), 4901-4906.
[28] Singh, S., Jha, P. K., Avdeev, M., Zhang, W., Jayanthi, K., Navrotsky, A., Alshareef, H. N., & Barpanda, P. (2021). Marinite Li2Ni(SO4)2 as a New Member of the Bisulfate Family of High-Voltage Lithium Battery Cathodes. *Chemistry of Materials, 33*(15), 6108-6119.
[29] Skoda, M., Dudek, I., Jarosz, A., & Szukiewicz, D. (2014). Graphene: One Material, Many Possibilities—Application Difficulties in Biological Systems. *Journal of Nanomaterials, 2014*, 890246.
[30] Zhang, S., Li, C., Zhang, X., Sun, X., Wang, K., & Ma, Y. (2017). High Performance Lithium-Ion Hybrid Capacitors Employing Fe3O4–Graphene Composite Anode and Activated Carbon Cathode. *ACS Applied Materials & Interfaces, 9*(20), 17136-17144.
[31] Pauling, L. (1931). The nature of the chemical bond. application of results obtained from the quantum mechanics and from a theory of paramagnetic susceptibility to the structure of molecules. *Journal of the American Chemical Society, 53*(4), 1367-1400.
[32] Mathur, R. B., Singh, B. P., & Pande, S. (2017). *Carbon nanomaterials: Synthesis, structure, properties and applications*. Taylor & Francis.
[33] Liao, Z., Gauquelin, N., Green, R. J., Macke, S., Gonnissen, J., Thomas, S., Zhong, Z., Li, L., Si, L., Van Aert, S., Hansmann, P., Held, K., Xia, J., Verbeeck, J., Van Tendeloo, G., Sawatzky, G. A., Koster, G., Huijben, M., & Rijnders, G. (2017). Thickness Dependent Properties in Oxide Heterostructures Driven by Structurally Induced Metal–Oxygen Hybridization Variations. *Advanced Functional Materials, 27*(17), 1606717.

[34] Kharisov, B. I., & Kharissova, O. V. (2019). *Carbon allotropes: Metal-complex chemistry, properties and applications.* Springer.
[35] Pérez, E. M., & Martín, N. (2015). π–π interactions in carbon nanostructures. *Chemical Society Reviews, 44*(18), 6425-6433.
[36] Novoselov, K. S., Geim, A. K., Morozov, S. V., Jiang, D., Zhang, Y., Dubonos, S. V., Grigorieva, I. V., & Firsov, A. A. (2004). Electric Field Effect in Atomically Thin Carbon Films. *Science, 306*(5696), 666-669.
[37] Clayden, J., Greeves, N., & Warren, S. G. (2012). *Organic Chemistry*. Oxford University Press.
[38] Yan, K., Peng, H., Zhou, Y., Li, H., & Liu, Z. (2011). Formation of Bilayer Bernal Graphene: Layer-by-Layer Epitaxy via Chemical Vapor Deposition. *Nano Letters, 11*(3), 1106-1110.
[39] Lee, J.-K., Kim, J.-G., Hembram, K. P. S. S., Kim, Y.-I., Min, B.-K., Park, Y., Lee, J.-K., Moon, D. J., Lee, W., Lee, S.-G., & John, P. (2016). The Nature of Metastable AA' Graphite: Low Dimensional Nano- and Single-Crystalline Forms. *Scientific Reports, 6*(1), 39624.
[40] Lee, J.-K., Lee, S., Kim, Y.-I., Kim, J.-G., Min, B.-K., Lee, K.-I., Park, Y., & John, P. (2014). The seeded growth of graphene. *Scientific Reports, 4*(1), 5682.
[41] Lee, J.-K., Lee, S., Kim, Y.-I., Kim, J.-G., Lee, K.-I., Ahn, J.-P., Min, B.-K., Yu, C.-J., Hwa Chae, K., & John, P. (2013). Structure of multi-wall carbon nanotubes: AA′ stacked graphene helices. *Applied Physics Letters, 102*(16), 161911.
[42] Zhang, F., Sahu, B., Min, H., & MacDonald, A. H. (2010). Band structure of ABC-stacked graphene trilayers. *Physical Review B, 82*(3), 035409.
[43] Baughman, R. H., Eckhardt, H., & Kertesz, M. (1987). Structure-property predictions for new planar forms of carbon: Layered phases containing sp2 and sp atoms. *The Journal of Chemical Physics*, *87*(11), 6687-6699.
[44] Li, G., Li, Y., Liu, H., Guo, Y., Li, Y., & Zhu, D. (2010). Architecture of graphdiyne nanoscale films. *Chemical Communications, 46*(19), 3256-3258.
[45] Yun, J., An, H., Huang, R., Guo, M., Zhang, Y., & Kang, P. (2020). Interesting Odd–Even Effect, Ohmic Contact, Negative Differential Resistance, and Current Stabilizer Behavior in All-Carbon Graphyne/Carbon-Chain Junctions. *IEEE Transactions on Electron Devices, 67*(6), 2529-2535.
[46] Jusélius, J., & Sundholm, D. (2001). The aromaticity and antiaromaticity of dehydroannulenes. *Physical Chemistry Chemical Physics, 3*(12), 2433-2437.
[47] Li, J., & Han, Y. (2023). Artificial carbon allotrope γ-graphyne: Synthesis, properties, and applications. *Giant*, *13*, 100140.
[48] Levine, I. N. (2014). *Quantum Chemistry*. Pearson.
[49] Lowe, J. P., & Peterson, K. A. (2006). *Quantum Chemistry*. Elsevier Academic Press.
[50] Mao, G.-Q., Yan, Z.-Y., Xue, K.-H., Ai, Z., Yang, S., Cui, H., Yuan, J.-H., Ren, T.-L., & Miao, X. (2022). DFT-1/2 and shell DFT-1/2 methods: electronic structure calculation for semiconductors at LDA complexity. *Journal of Physics: Condensed Matter*, *34*(40), 403001.
[51] Sabe, V. T., Ntombela, T., Jhamba, L. A., Maguire, G. E. M., Govender, T., Naicker, T., & Kruger, H. G. (2021). Current trends in computer aided drug design and a highlight of drugs discovered via computational techniques: A review. *European Journal of Medicinal Chemistry*, *224*, 113705.
[52] Dias, R. E., & Magalhaes, A. L. (2024). Unveiling the potential of graphene and graphyne electrodes in lithium-ion batteries: A DFT modeling approach. *Computational and Theoretical Chemistry*, *1233*, 114494.
[53] Jensen, F. (2017). *Introduction to computational chemistry*. John Wiley & Sons, Ltd.
[54] Hohenberg, P., & Kohn, W. (1964). Inhomogeneous Electron Gas. *Physical Review, 136*(3B), B864-B871.

[55] Gaussian 16, Revision C.01, Frisch, M. J.; Trucks, G. W.; Schlegel, H. B.; Scuseria, G. E.; Robb, M. A.; Cheeseman, J. R.; Scalmani, G.; Barone, V.; Petersson, G. A.; Nakatsuji, H.; Li, X.; Caricato, M.; Marenich, A. V.; Bloino, J.; Janesko, B. G.; Gomperts, R.; Mennucci, B.; Hratchian, H. P.; Ortiz, J. V.; Izmaylov, A. F.; Sonnenberg, J. L.; Williams-Young, D.; Ding, F.; Lipparini, F.; Egidi, F.; Goings, J.; Peng, B.; Petrone, A.; Henderson, T.; Ranasinghe, D.; Zakrzewski, V. G.; Gao, J.; Rega, N.; Zheng, G.; Liang, W.; Hada, M.; Ehara, M.; Toyota, K.; Fukuda, R.; Hasegawa, J.; Ishida, M.; Nakajima, T.; Honda, Y.; Kitao, O.; Nakai, H.; Vreven, T.; Throssell, K.; Montgomery, J. A., Jr.; Peralta, J. E.; Ogliaro, F.; Bearpark, M. J.; Heyd, J. J.; Brothers, E. N.; Kudin, K. N.; Staroverov, V. N.; Keith, T. A.; Kobayashi, R.; Normand, J.; Raghavachari, K.; Rendell, A. P.; Burant, J. C.; Iyengar, S. S.; Tomasi, J.; Cossi, M.; Millam, J. M.; Klene, M.; Adamo, C.; Cammi, R.; Ochterski, J. W.; Martin, R. L.; Morokuma, K.; Farkas, O.; Foresman, J. B.; Fox, D. J. Gaussian, Inc., Wallingford CT, 2016.
[56] Koch, W., & Holthausen, M. C. (2001). *A chemist's guide to density functional theory.* Wiley-VCH.
[57] Becke, A. D. (2014). Perspective: Fifty years of density-functional theory in chemical physics. *The Journal of Chemical Physics, 140*(18), 18A301.
[58] Yu, H. S., He, X., Li, S. L., & Truhlar, D. G. (2016). MN15: A Kohn–Sham global-hybrid exchange–correlation density functional with broad accuracy for multi-reference and single-reference systems and noncovalent interactions. *Chemical Science, 7*(8), 5032-5051.
[59] Francl, M. M., Pietro, W. J., Hehre, W. J., Binkley, J. S., Gordon, M. S., DeFrees, D. J., & Pople, J. A. (1982). Self-consistent molecular orbital methods. XXIII. A polarization-type basis set for second-row elements. *The Journal of Chemical Physics*, *77*(7), 3654-3665.
[60] Petersson, G. A., Bennett, A., Tensfeldt, T. G., Al-Laham, M. A., Shirley, W. A., & Mantzaris, J. (1988). A complete basis set model chemistry. I. The total energies of closed-shell atoms and hydrides of the first-row elements. *The Journal of Chemical Physics*, *89*(4), 2193-2218.
[61] Petersson, G. A., & Al-Laham, M. A. (1991). A complete basis set model chemistry. II. Open-shell systems and the total energies of the first-row atoms. *The Journal of Chemical Physics*, *94*(9), 6081-6090.
[62] Xu, K. (2004). Nonaqueous Liquid Electrolytes for Lithium-Based Rechargeable Batteries. *Chemical Reviews*, *104*(10), 4303-4418.
[63] Ravikumar, B., Mynam, M., Repaka, S., & Rai, B. (2021). Solvation shell dynamics explains charge transport characteristics of LIB electrolytes. *Journal of Molecular Liquids*, *338*, 116613.
[64] Borodin, O., & Smith, G. D. (2009). Quantum Chemistry and Molecular Dynamics Simulation Study of Dimethyl Carbonate: Ethylene Carbonate Electrolytes Doped with LiPF6. *The Journal of Physical Chemistry B*, *113*(6), 1763-1776.
[65] Kim, J. Y., Shin, D. O., Chang, T., Kim, K. M., Jeong, J., Park, J., Lee, Y. M., Cho, K. Y., Phatak, C., Hong, S., & Lee, Y.-G. (2019). Effect of the dielectric constant of a liquid electrolyte on lithium metal anodes. *Electrochimica Acta*, *300*, 299-305.
[66] Scalmani, G., & Frisch, M. J. (2010). Continuous surface charge polarizable continuum models of solvation. I. General formalism. *The Journal of Chemical Physics*, *132*(11), 114110.
[67] Daniels, I. N., Wang, Z., & Laird, B. B. (2017). Dielectric Properties of Organic Solvents in an Electric Field. *The Journal of Physical Chemistry C*, *121*(2), 1025-1031.
[68] Mehra, R. (2003). Application of refractive index mixing rules in binary systems of hexadecane and heptadecane with n-alkanols at different temperatures. *Journal of Chemical Sciences, 115*, 147-154.
[69] Naejus, R., Lemordant, D., Coudert, R., & Willmann, P. (1997). Excess thermodynamic properties of binary mixtures containing linear or cyclic carbonates as

solvents at the temperatures 298.15 K and 315.15 K. *The Journal of Chemical Thermodynamics*, *29*(12), 1503-1515.
[70] Peppel, W. J. (1958). Preparation and Properties of the Alkylene Carbonates. *Industrial & Engineering Chemistry*, *50*(5), 767-770.
[71] Moosavi, M., Motahari, A., Vahid, A., Akbar, V., Rostami, A. A., & Omrani, A. (2016). Densities, Viscosities, and Refractive Indices of Dimethyl Carbonate + 1-Hexanol/1-Octanol Binary Mixtures at Different Temperatures. *Journal of Chemical & Engineering Data*, *61*(6), 1981-1991.
[72] Jaguar. (2015). Jaguar 8.8 User Manuel. Schrödinger Press. http://gohom.win/ManualHom/Schrodinger/Schrodinger_2015-2_docs/jaguar/jaguar_user_manual.pdf, Accessed 4 May 2022.
[73] Lim, T. M., Menictas, C., & Skyllas-Kazacos, M. (2015). *Advances in batteries for medium- and large-scale energy storage.* Woodhead Publishing.
[74] Trasatti, S. (2009). Electrochemical theory | Electrokinetics. In J. Garche (Ed.), *Encyclopedia of Electrochemical Power Sources* (pp. 23-31). Elsevier.
[75] Rocchini, G. (1996). A theoretical study of the influence of the ohmic drop on polarization curves. *Corrosion Science*, *38*(4), 655-668.
[76] Bard, A. J., & Faulkner, L. R. (2000). *Electrochemical methods: Fundamentals and applications*. Wiley.
[77] Winget, P., Weber, E. J., Cramer, C. J., & Truhlar, D. G. (2000). Computational electrochemistry: aqueous one-electron oxidation potentials for substituted anilines *Physical Chemistry Chemical Physics*, *2*(6), 1231-1239.
[78] Winget, P., Cramer, C. J., & Truhlar, D. G. (2004). Computation of equilibrium oxidation and reduction potentials for reversible and dissociative electron-transfer reactions in solution. *Theoretical Chemistry Accounts*, *112*(4), 217-227.
[79] Shriver, D. F., & Atkins, P. W. (2006). Inorganic Chemistry. Oxford University Press.
[80] The absolute electrode potential: an explanatory note (Recommendations 1986). (1986). *Journal of Electroanalytical Chemistry and Interfacial Electrochemistry*, *209*(2), 417-428.
[81] Go, C. Y., Jeong, G. S., & Kim, K. C. (2019). Pyrenetetrone Derivatives Tailored by Nitrogen Dopants for High-Potential Cathodes in Lithium-Ion Batteries. *iScience*, *21*, 206-216.
[82] Kim, S., Kim, K. C., Lee, S. W., & Jang, S. S. (2016). Thermodynamic and redox properties of graphene oxides for lithium-ion battery applications: a first principles density functional theory modeling approach. *Physical Chemistry Chemical Physics*, *18*(30), 20600-20606.
[83] Yu, H. S., He, X., Li, S. L., & Truhlar, D. G. (2016). MN15: A Kohn–Sham global-hybrid exchange–correlation density functional with broad accuracy for multi-reference and single-reference systems and noncovalent interactions. *Chemical Science*, *7*(8), 5032-5051.
[84] Jinnouchi, R., & Anderson, A. B. (2008). Aqueous and Surface Redox Potentials from Self-Consistently Determined Gibbs Energies. *The Journal of Physical Chemistry C*, *112*(24), 8747-8750.
[85] Winget, P., Cramer, C. J., & Truhlar, D. G. (2004). Computation of equilibrium oxidation and reduction potentials for reversible and dissociative electron-transfer reactions in solution. *Theoretical Chemistry Accounts*, *112*(4), 217-227.
[86] Winget, P., Weber, E. J., Cramer, C. J., & Truhlar, D. G. (2000). Computational electrochemistry: aqueous one-electron oxidation potentials for substituted anilines. *Physical Chemistry Chemical Physics*, *2*(6), 1231-1239.

Appendix 1

Table 1

Parameters of the mixtures used in the PCM calculations and properties of EC and DMC pure liquids and mixtures at 313.15 K.

Properties	Pure EC	Pure DMC	8:2 EC/DMC
Molar mass/gmol^{-1}	88.06	90.08	88.46
Density/gcm^{-3}	1.322[73]	1.041[73]	1.257[37]
Molar volume/cm^{3}mol^{-1}	66.71	86.62	*
Volume ratio	1	1	7.5:2.5
Refractive index	1.416[74]	1.370[75]	1.185
Molecular mass/g	1.46×10^{-22}	1.50×10^{-22}	8.85×10^{-22}
Packing density	**	**	**
Static dielectric constant	90.03[73]	3.19[73]	62.43[73]
Dynamic dielectric constant	2.004	1.877	1.380
Solvent radius/Å	2.36	2.58	2.41

*Property not needed for calculations.

**Values of packing densities were assumed to be 0.5, otherwise a detailed data of the crystal structure of the liquids would be required [72].

Appendix 2

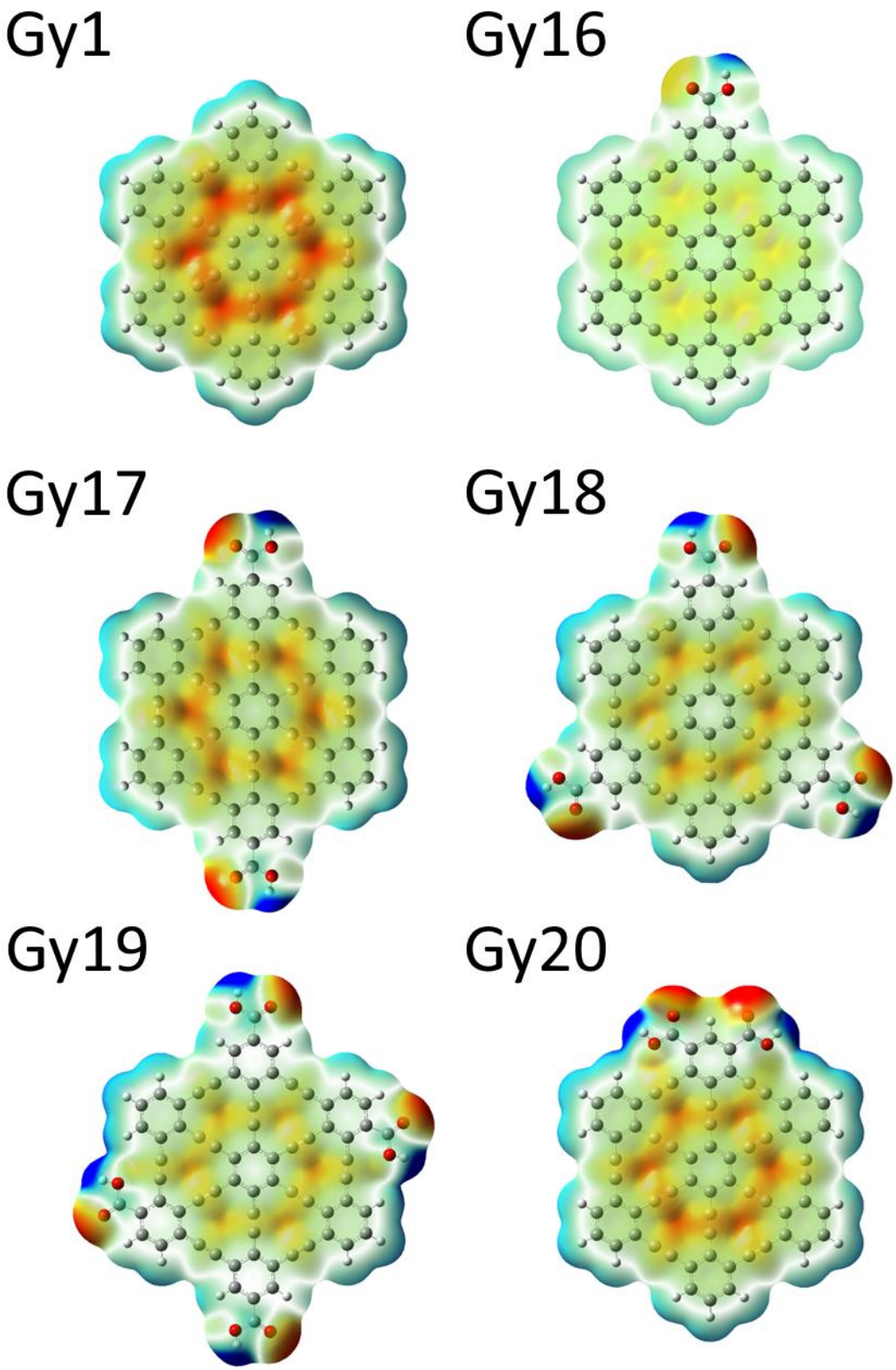

Figure 1: Surface charge distribution for Gy1, Gy16, Gy17, Gy18, Gy19 and Gy20.

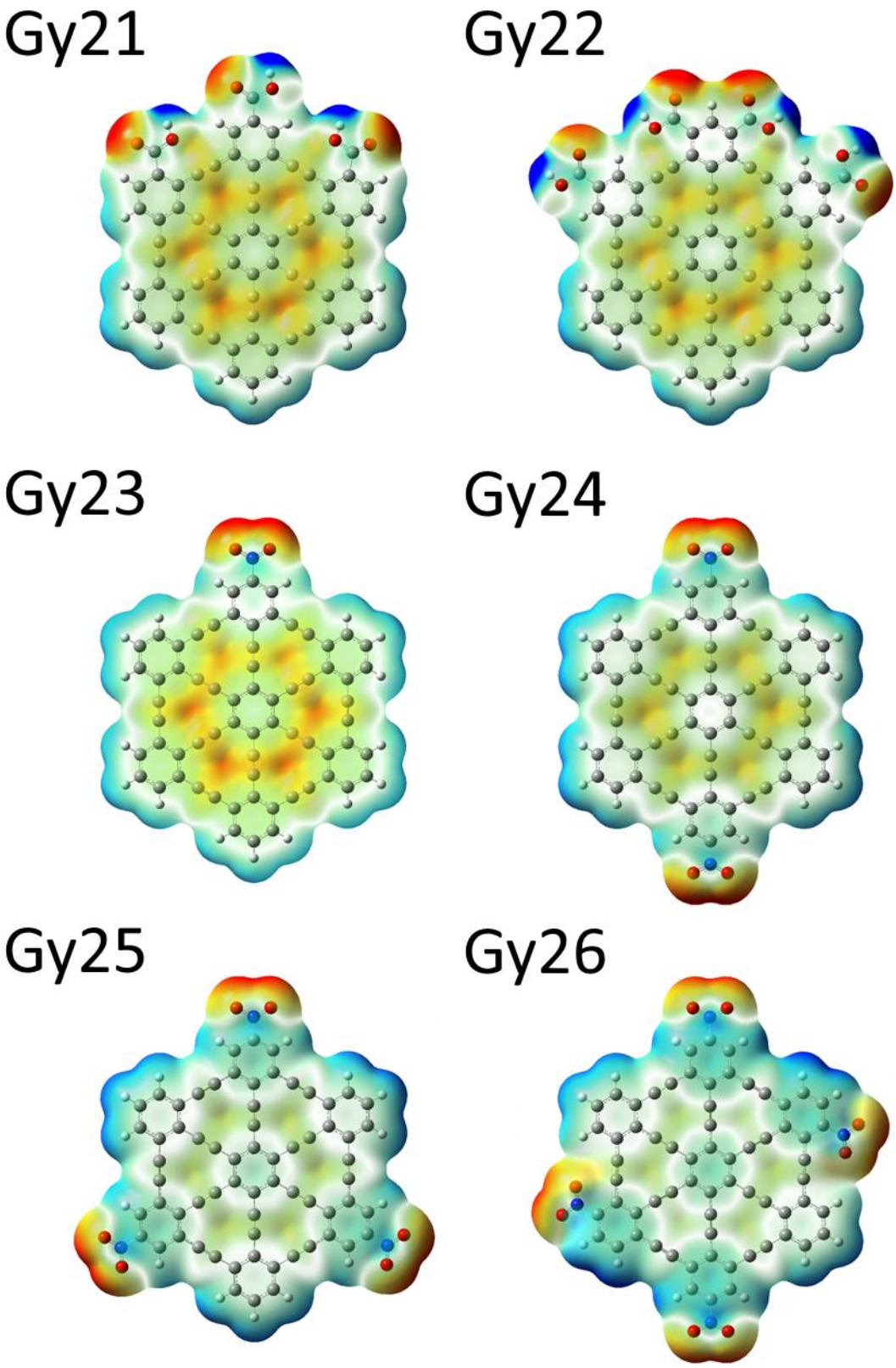

Figure 2: Surface charge distribution for Gy21, Gy22, Gy23, Gy24, Gy25 and Gy26.

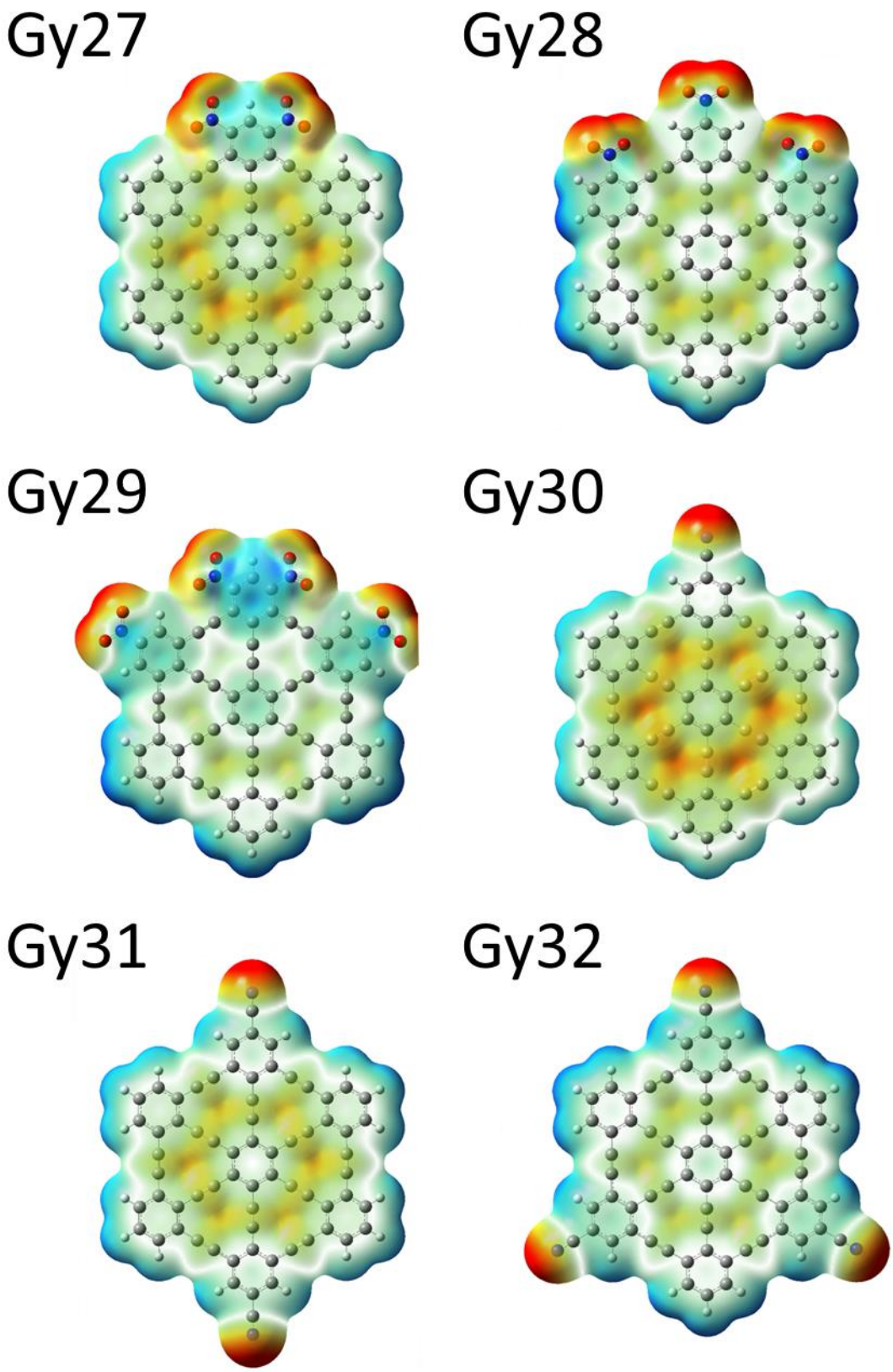

Figure 3: Surface charge distribution for Gy27, Gy28, Gy29, Gy30, Gy31 and Gy32.

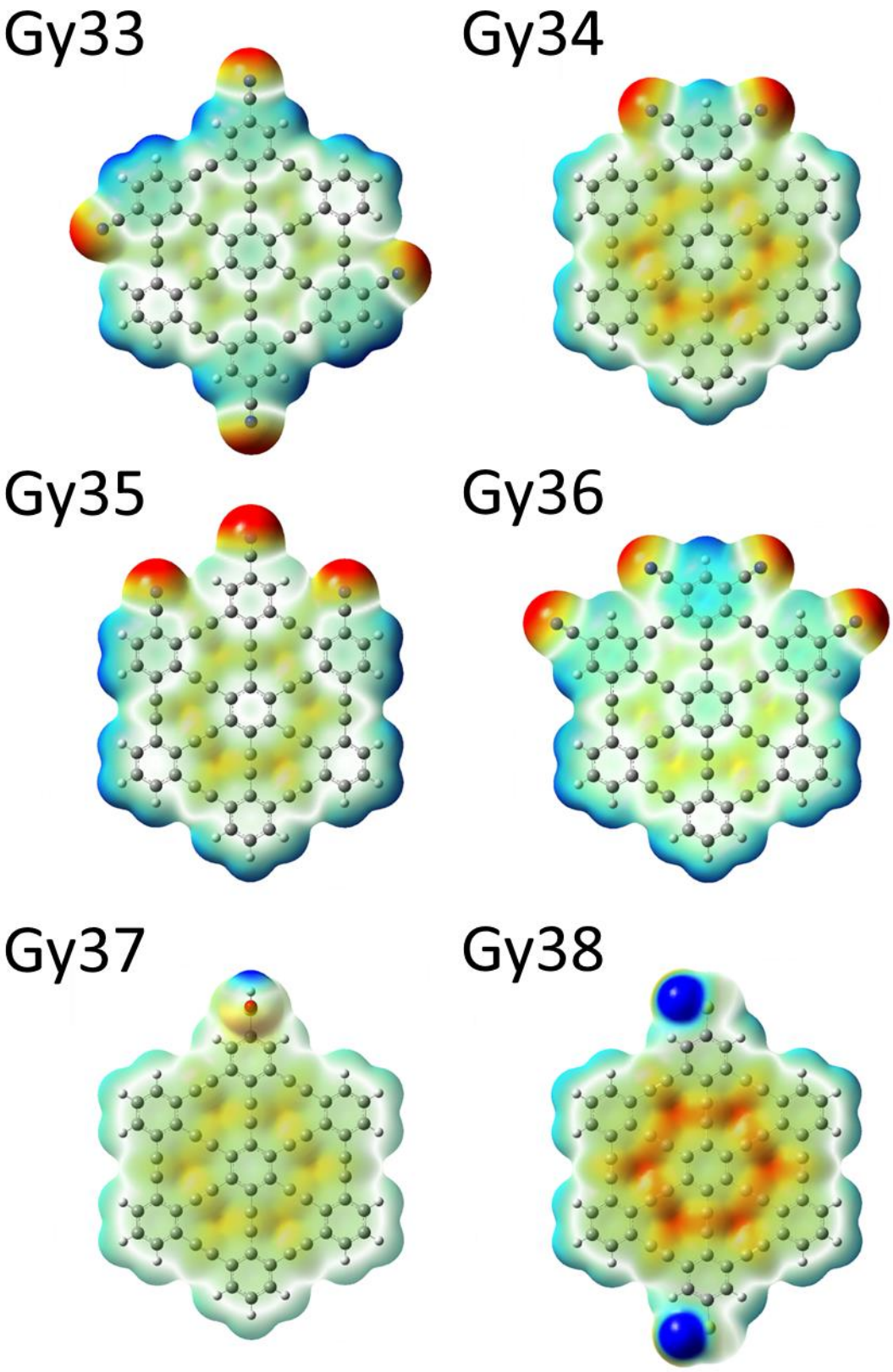

Figure 4: Surface charge distribution for Gy33, Gy34, Gy35, Gy36, Gy37 and Gy38.

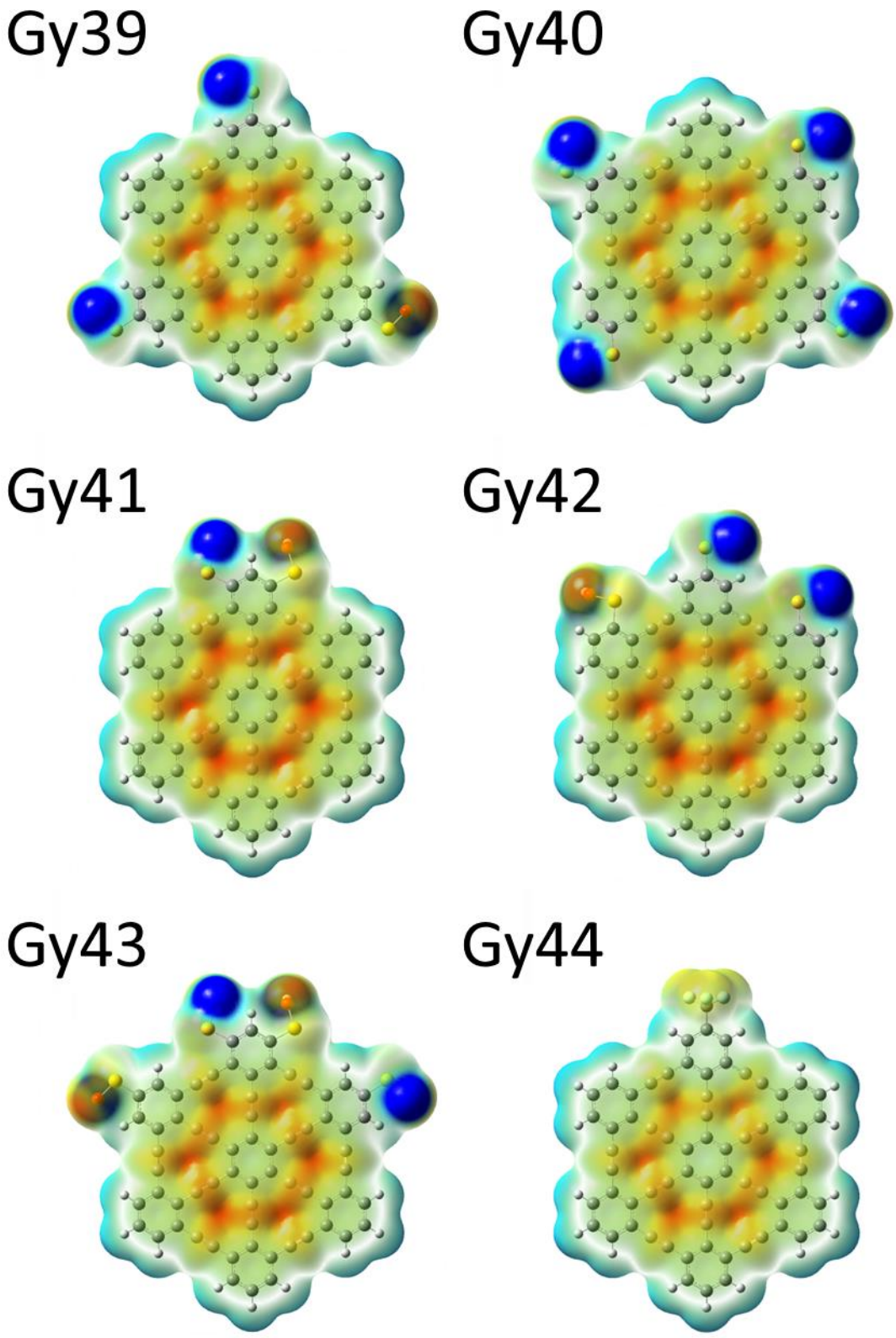

Figure 5: Surface charge distribution for Gy39, Gy40, Gy41, Gy42, Gy43 and Gy44.

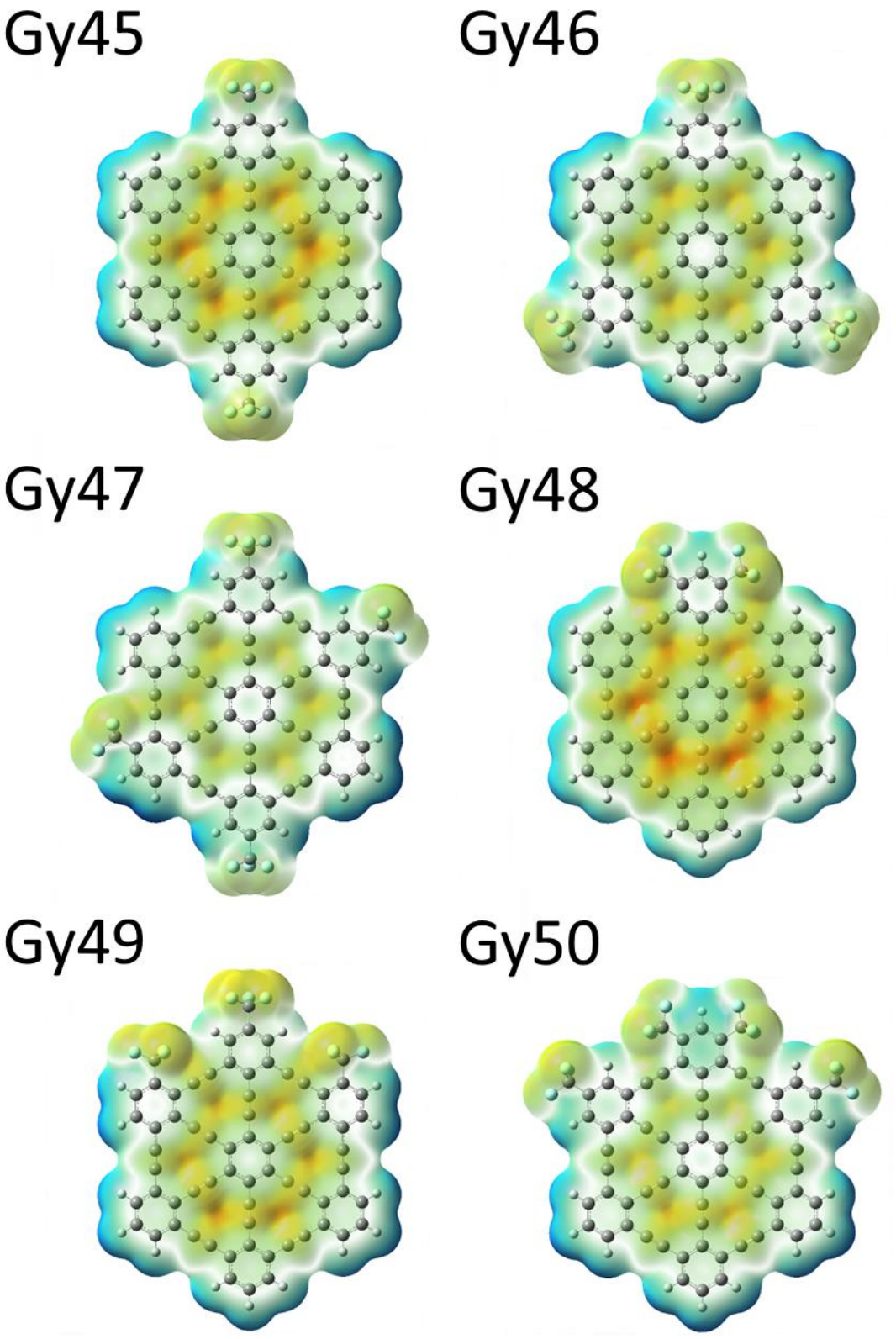

Figure 6: Surface charge distribution for Gy45, Gy46, Gy47, Gy48, Gy49 and Gy50.

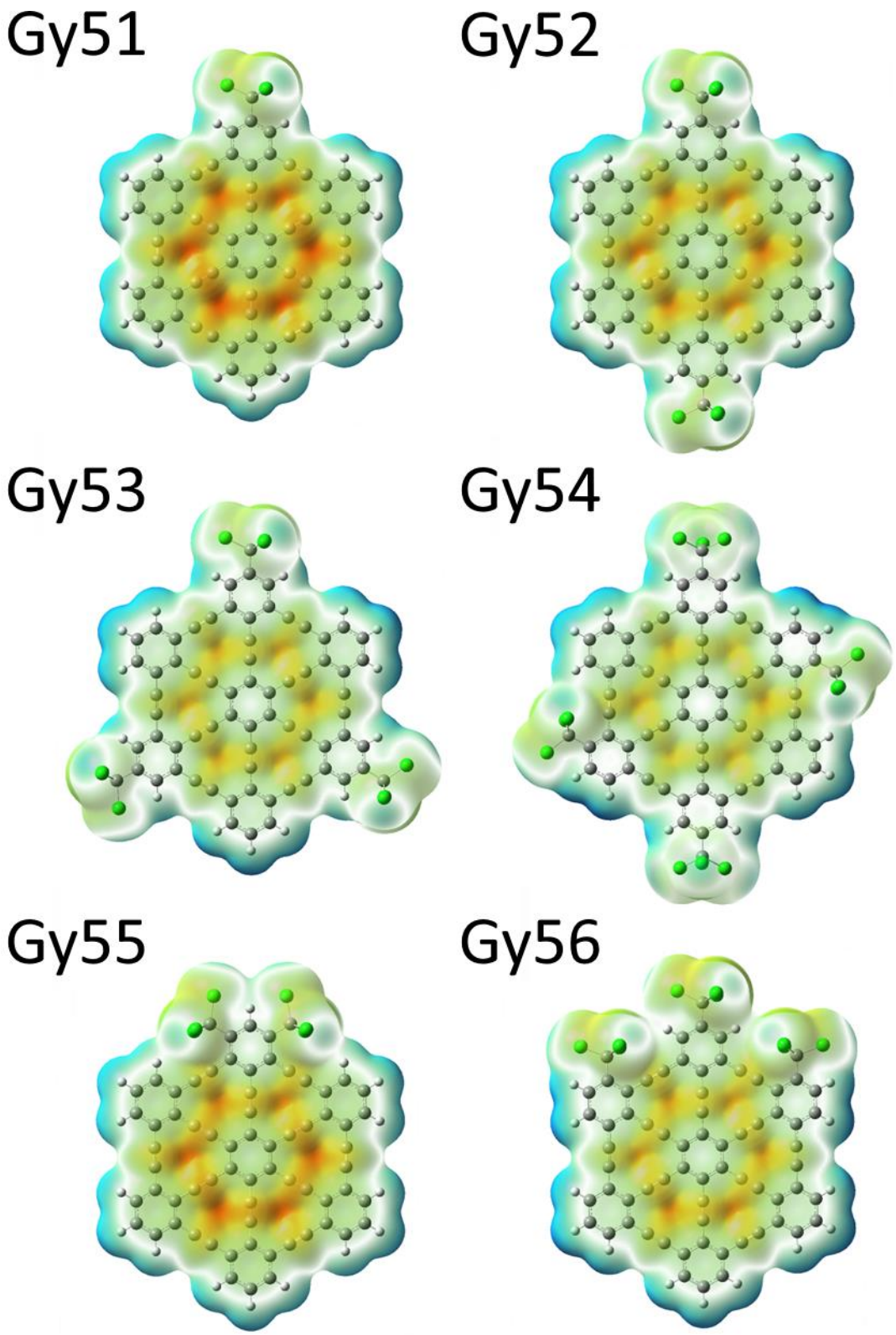

Figure 7: Surface charge distribution for Gy51, Gy52, Gy53, Gy54, Gy55 and Gy56.

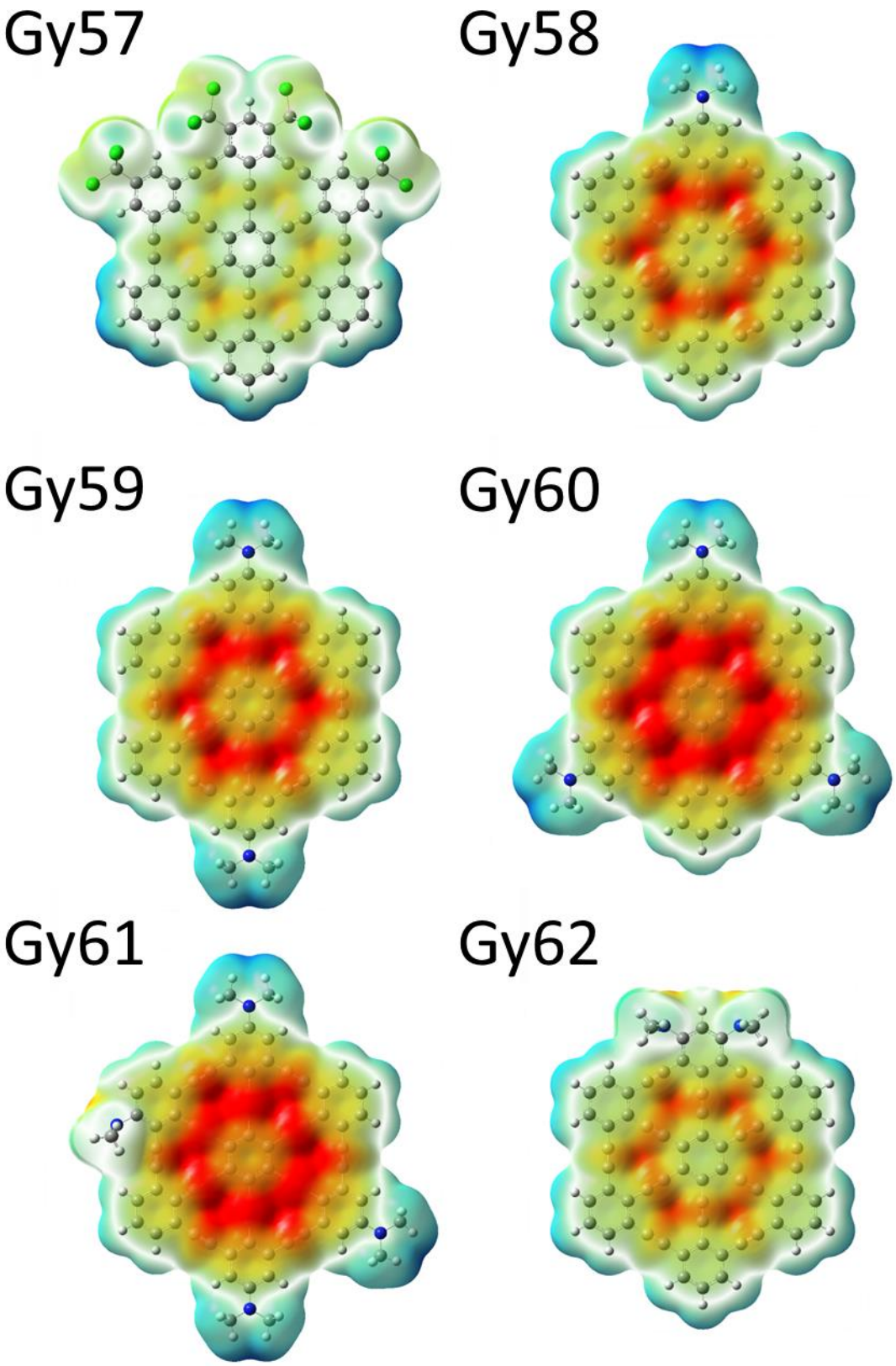

Figure 8: Surface charge distribution for Gy57, Gy58, Gy59, Gy60, Gy61 and Gy62.

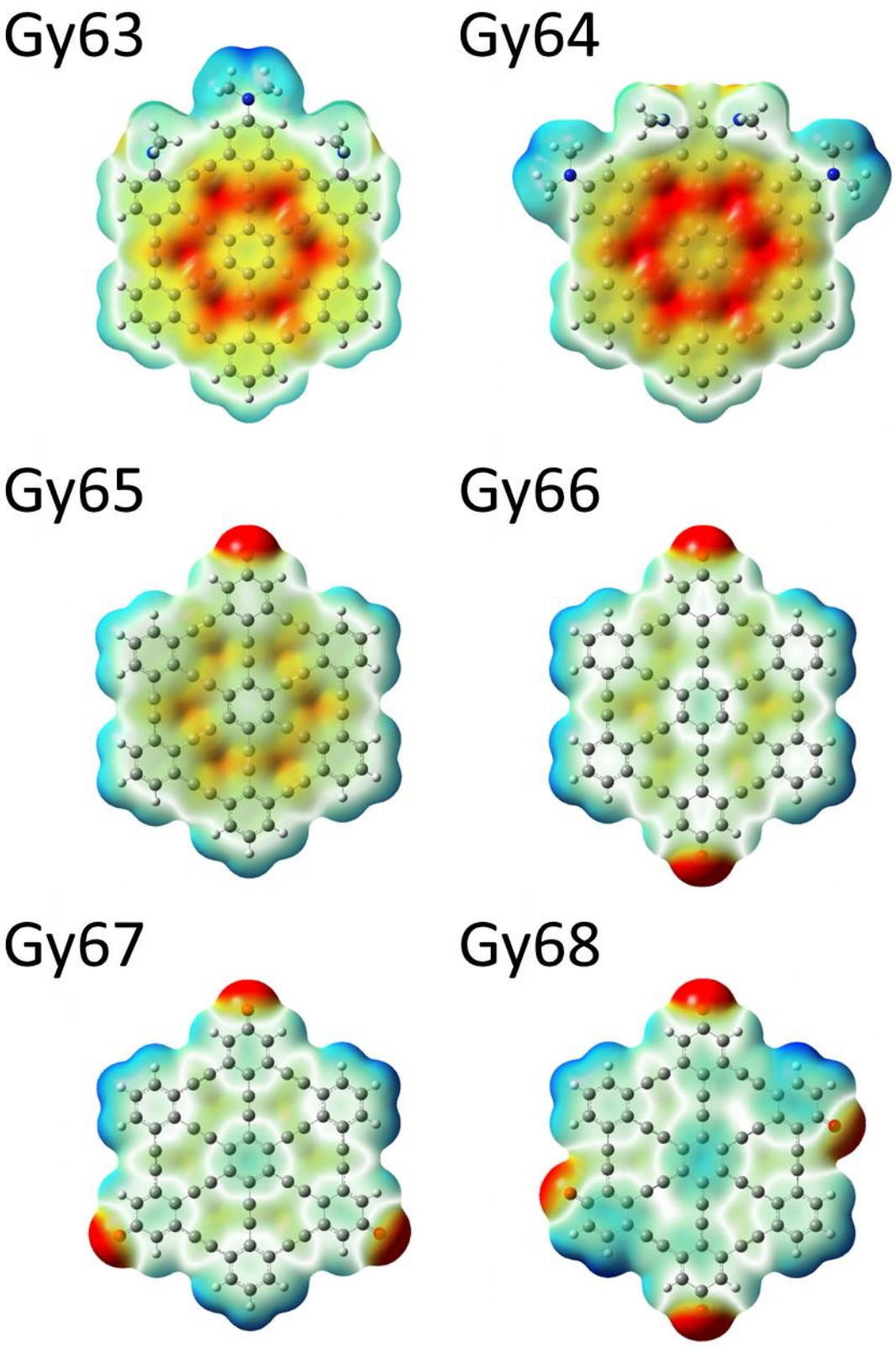

Figure 9: Surface charge distribution for Gy63, Gy64, Gy65, Gy66, Gy67 and Gy68.

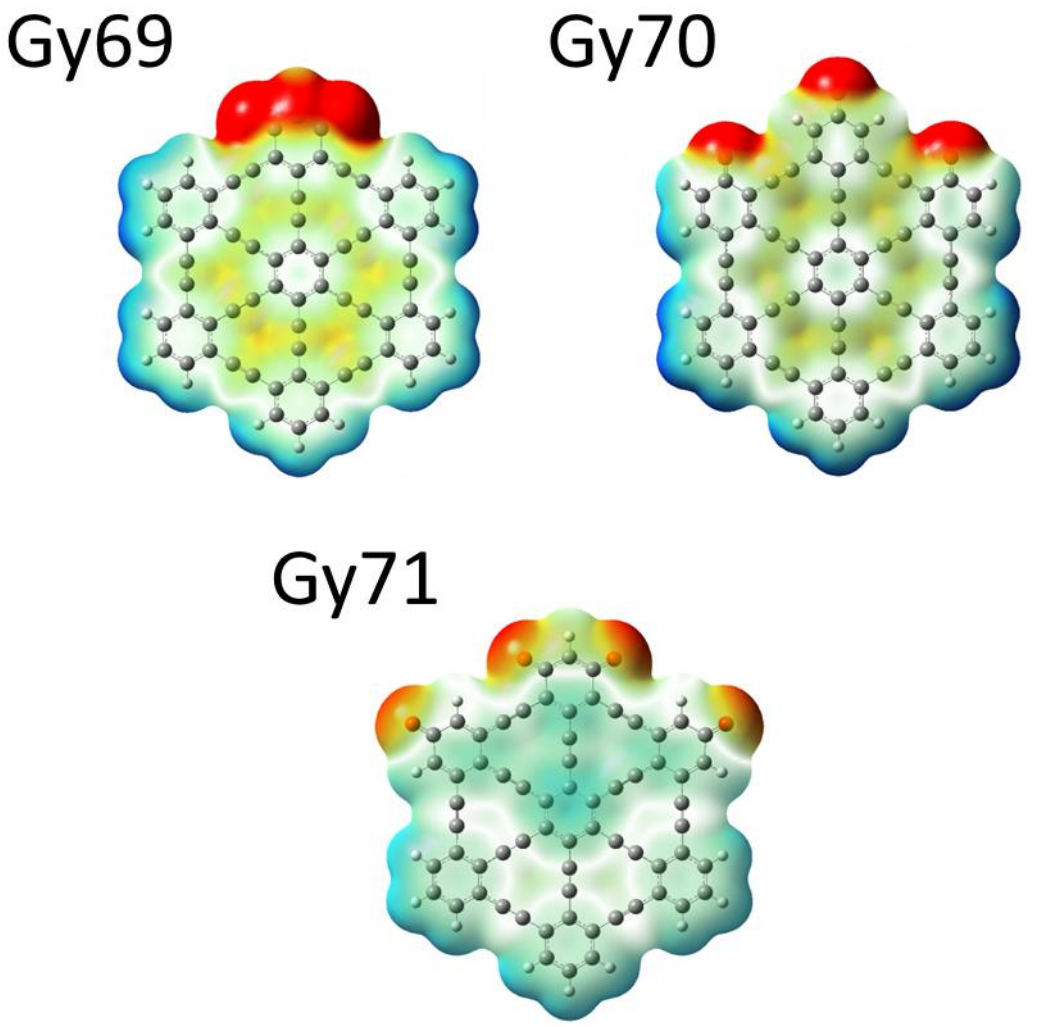

Figure 10: Surface charge distribution for Gy69, Gy70 and Gy71.